Helsinki University of Technology Control Engineering Laboratory

Espoo 2006 Report 149

MODELLING, ESTIMATION AND CONTROL OF ELECTROLESS NICKEL PLATING PROCESS OF PRINTED CIRCUIT BOARD MANUFACTURING

Kalle Kantola

TEKNILLINEN KORKEAKOULU
TEKNISKA HÖGSKOLAN
HELSINKI UNIVERSITY OF TECHNOLOGY
TECHNISCHE UNIVERSITÄT HELSINKI
UNIVERSITE DE TECHNOLOGIE D´HELSINKI

Helsinki University of Technology Control Engineering Laboratory

Espoo March 2006 Report 149

MODELLING, ESTIMATION AND CONTROL OF ELECTROLESS NICKEL PLATING PROCESS OF PRINTED CIRCUIT BOARD MANUFACTURING

Kalle Kantola

Dissertation for the degree of Doctor of Science in Technology to be presented with due permission of the Department of Automation and Systems Technology, for public examination and debate in Auditorium AS1 at Helsinki University of Technology (Espoo, Finland) on the 17th of November, 2006, at 12 noon.

Helsinki University of Technology

Department of Automation and Systems Technology

Control Engineering Laboratory

Distribution:
Helsinki University of Technology
Control Engineering Laboratory
P.O. Box 5500
FI-02015 HUT, Finland
Tel. +358-9-451 5201
Fax. +358-9-451 5208
E-mail: control.engineering@tkk.fi
http://www.control.tkk.fi/

ISBN-13 978-951-22- 8440-5 (printed)
ISBN-10 951-22-8440-5 (printed)
ISBN-13 978-951-22- 8441-2 (pdf)
ISBN-10 951-22- 8441-3 (pdf)
ISSN 0356-0872

Picaset Oy
Helsinki 2006

Available on net at http://lib.tkk.fi/Diss/2006/isbn9512284413

HELSINKI UNIVERSITY OF TECHNOLOGY P. O. BOX 1000, FI-02015 TKK http://www.tkk.fi	ABSTRACT OF DOCTORAL DISSERTATION

Author Kalle Kantola

Name of the dissertation

Modelling, Estimation and Control of Electroless Nickel Plating Process of Printed Circuit Board Manufacturing

Date of manuscript 3.3.2006	Date of the dissertation 17.11.2006
[X] Monograph	[ ] Article dissertation (summary + original articles)

Department	Automation and Control Engineering
Laboratory	Control Engineering Laboratory
Field of research	Process control
Opponent(s)	Professor Kauko Leiviskä, Docent Jarmo Määttänen
Supervisor	Professor Heikki Koivo
(Instructor)	Docent Robert Tenno

Abstract

Electroless nickel plating is a part of electroless nickel immersion gold (ENIG)-surface finish used in printed circuit board (PCB) manufacturing. In the ENIG-surface finish, the electroless nickel alloy prevents the oxidation of a circuitry by working as a diffusion barrier between the coppered circuitry and protective gold alloy and protecting the circuitry from mechanical tearing.

It is well-known that the thickness and phosphorous content of the electroless nickel alloy have a dramatic effect on the PCB's characteristics. Unfortunately, these parameters cannot be directly measured during the plating process which makes it impossible to control the parameters in traditional way.

In this thesis a new model for electroless nickel plating process is developed using electrochemical reaction mechanism and mixed potential theory. The model inputs are the standard online measurements of PCB plating line. From these the model produces accurate realtime estimates *inter alia* from alloy thickness, phosphorous content, by-product concentrations and current densities of partial reactions. The developed model has been tested against independent data gathered from three active and several passive experiments conducted in an industrial PCB manufacturing line. In all the experiments, the model shows good agreement with the data and correct response to the changes in plating conditions. The behavior of the model is in a good agreement with the literature and former research results.

It the thesis, the model is applied in model-based monitoring of an industrial plating process and it is shown to be capable of estimating online the unobservable product and electrical process parameters from standard measurements of PCB-industry.

Based on the model also a new sophisticated control algorithm is developed. The algorithm calculates the optimal nickel ion concentration and pH trajectories by which the desired alloy thickness and phosphorous content are reached. These trajectories are tracked by PI-controlled pumping of ammonia and nickel sulphate. The performance of the control algorithm is tested by simulation and it is shown to be effective.

Keywords	Electroless nickel, printed circuit board manufacturing, modelling, estimation, process control	
ISBN (printed)	951-22-8440-5	ISSN (printed) 0356-0872
ISBN (pdf)	951-22-8441-3	ISSN (pdf)
ISBN (others)		Number of pages 83
Publisher	Helsinki University of Technology, Control Engineering Laboratory	
Print distribution	Helsinki University of Technology, Control Engineering Laboratory	
[X] The dissertation can be read at http://lib.tkk.fi/Diss/		

TEKNILLINEN KORKEAKOULU
PL 1000, 02015 TKK
http://www.tkk.fi

VÄITÖSKIRJAN TIIVISTELMÄ

Tekijä Kalle Kantola

Väitöskirjan nimi

Piirilevyjen valmistuksessa käytettävän autokatalyyttisen nikkelipinnoitusprosessin mallinnus, estimointi ja säätö

Käsikirjoituksen jättämispäivämäärä 3.3.2006 | Väitöstilaisuuden ajankohta 17.11.2006

[X] Monografia [ ] Yhdistelmäväitöskirja (yhteenveto + erillisartikkelit)

Osasto Automaatio- ja systeemitekniikka
Laboratorio Systeemitekniikan laboratorio
Tutkimusala Prosessisäätö
Vastaväittäjä(t) Professori Kauko Leiviskä, Dosentti Jarmo Määttänen
Työn valvoja Professori Heikki Koivo
(Työn ohjaaja) Dosentti Robert Tenno

Tiivistelmä

Autokatalyyttinen nikkelipinnoitus on osa piirilevyjen valmistuksessa käytettävää nikkeli-kulta -pintaviimeistelyä. Tässä prosessissa autokatalyytinen nikkeli suojaa virtapiiriä hapettumiselta estämällä diffuusion kuparisen virtapiirin ja suojaavan kultaisen pintakerroksen välissä. Samalla nikkelikerros parantaa virtapiirin kulutuskestävyyttä.

On yleisesti tiedettyä, että autokatalyyttisen nikkelikerroksen paksuudella ja fosforipitoisuudella on kriittinen vaikutus piirilevyn laadullisiin ominaisuuksiin. Valitettavasti näitä parametreja ei voida mitata reaaliaikaisesti pinnoitusprosessin aikana, mikä tekee perinteisen prosessisäädön hyödyntämisen mahdottomaksi.

Tässä väitöskirjassa on kehitetty uusi malli kuvaamaan autokatalyyttistä nikkelipinnoitusprosessia. Malli perustuu elektrokemialliseen reaktiomekanismiin ja ns. sekapotenttiaaliteoriaan. Mallin syötteenä ovat piirilevyjen tuotantolinjan standardit, reaaliaikaiset prosessimittaukset, joiden perusteella malli tuottaa reaaliaikaiset estimaatit mm. kerrospaksuudesta, fosforipitoisuudesta, sivutuotteiden konsentraatioista ja osittaisreaktioiden virrantiheyksistä. Kehitetyn mallin tarkkuutta on testattu teollisesta tuotantolinjasta mitatulla riippumattomalla mittausaineistolla. Testien perusteella mallin on todettu olevan tarkka ja sen vasteet eri olosuhteidenmuutoksiin oikeita.

Malliin perustuen on väitöskirjassa kehitetty mallipohjainen monitorointialgoritmi autokatalyytisen nikkelipinnoitusprosessin ohjaamiseen. Monitorointialgoritmia on testattu riippumattomalla mittausaineistolla ja sen on osoitettu kykenevän ennustamaan reaaliaikaisesti ei-mitattavat tuote- ja prosessiparametrit standardeista prosessimittauksista.

Kehitettyyn malliin perustuen on väitöskirjassa kehitetty myös uusi säätöalgoritmi. Algoritmi laskee mallin avulla optimaaliset trajektorit pinnoituskylvyn nikkeli-ioni konsentraatiolle ja pH-indeksille annettujen tavoitekerropaksuuden ja -fosforipitoisuuden perusteella. Kylvyn pitoisuudet saatetaan trajektorien määräämälle tasollle PI-säädettyjen ammoniakki ja nikkelisulfaattipumppausten avulla. Säätöalgoritmi on osoitettu tehokkaaksi suoritettujen simulointien perusteella.

Asiasanat Autokatalyytinen nikkeli, piirilevyjen valmistus, mallinnus, estimointi, prosessisäätö

ISBN (painettu) 951-22-8440-5	ISSN (painettu) 0356-0872
ISBN (pdf) 951-22-8441-3	ISSN (pdf)
ISBN (muut)	Sivumäärä 83

Julkaisija Teknillinen korkeakoulu, Systeemitekniikan laboratorio

Painetun väitöskirjan jakelu Teknillinen korkeakoulu, Systeemitekniikan laboratorio

[X] Luettavissa verkossa osoitteessa http://lib.tkk.fi/Diss/

Preface

This dissertation was carried out in the Control Engineering Laboratory at Helsinki University of Technology. I wish to express my sincere gratitude to my instructor Docent Robert Tenno, who introduced me to the topic and who had always time for discussions with me. Also my supervisor Professor Heikki Koivo deserves my best compliments because of his encouragement and sincere belief in me and my work. Several persons have helped me during the test phase of the research. The assistance of Mrs. Lotta Ekebom, Mrs. Tarja Rapala-Virtanen, Mrs. Juulia Loisa, Dr. Jukka Ranta and Mr. Jani Kaartinen during different phases of the tests has been of indispensable help.

During the research, financial support has been provided by the Finnish Academy Graduate school in Electronics, Telecommunications and Automation (GETA), Emil Aaltonen Foundation, Jenny and Antti Wihuri Foundation, the Finnish Cultural Foundation, the Finnish Society of Automation, the Scandinavia-Japan Sasakawa Foundation and the Technology Promotion Foundation. This support is gratefully acknowledged.

Finally I thank the whole personnel of the Control Engineering Laboratory. Since I became a researcher, I have felt like being a part of a family.

Nagoya, Japan. August 2006

Kalle Kantola

Nomenclature

Symbols

A	-	bath loading (total area immersed per bath volume), cm^2/dm^3
A_p	-	maximum loading, dm^2/dm^3
C_{Ni}	-	volumetric charge density of nickel, C/cm^3
C_P	-	volumetric charge density of phosphorous, C/cm^3
c_1	-	hypophosphite concentration, $molH_2PO_2^-/dm^3$
c_3	-	hydrogen ion concentration, $mol\ H^+/dm^3$
c_4	-	nickel concentration, $molNi^{2+}/cm^3$
c_5	-	sulphate concentration, $mol\ SO_4^{2-}/dm^3$
c_6	-	ammonia concentration, $mol\ NH_3/dm^3$
c_7	-	ammonium concentration, $mol\ NH_4^+/dm^3$
c_8	-	orthophosphite concentration, $molH_2PO_3^-/dm^3$
c_9	-	ammonium sulphate concentration, $mol\ [NH_4]_2SO_4/dm^3$
c_{10}	-	hydrogen gas concentration, $mol\ H_2(g)/dm^3$
c_{1f}	-	feeding concentration of hypophosphite, $mol\ H_2PO_2^-/dm^3$
c_{3f}	-	feeding concentration of ammonia, $mol\ NH_3/dm^3$
c_{4f}	-	feeding concentration of nickel sulphate, $molNi^{2+}/dm^3$
c_{5max}	-	maximum concentration of sulphate, mol/dm^3
c_{1ref}	-	reference concentration of hypophosphite, mol/dm^3
c_{3ref}	-	reference concentration of hydrogen ion, mol/dm^3
c_{4ref}	-	reference concentration of nickel ion, mol/dm^3
dx_3	-	dissociation-consumed hydrogen, $mol\ H^+/dm^3$
dx_6	-	dissociation-consumed ammonia, $mol\ NH_3/dm^3$
dx_7	-	dissociation-produced ammonium, $mol\ NH_4^+/dm^3$
F	-	Faraday's constant, 96487 C/mol
J	-	vector of cost functions, $J = [J_3, J_4]^T$
J_3	-	cost function of pH
J_4	-	cost function of nickel percentage

i_1 - current density of oxidation reaction, A/cm^2
i_2 - current density of phosphorous deposition reaction, A/cm^2
i_3 - current density of hydrogen gas evolution reaction, A/cm^2
i_4 - current density of nickel deposition reaction, A/cm^2
K_P - control gain, diagonal matrix of weights
k - temperature voltage, $k = F/RT$, $1/V$
M_{Ni} - molecular weight of nickel, g/mol
M_P - molecular weight of phosphorous, g/mol
p_n - number of exchanged electrons, $p_1 = p_3 = p_4 = 2$, $p_2 = 1$
Q_{1f} - hypophosphite feeding rate, $1/s$
Q_{3f} - ammonia feeding rate, $1/s$
Q_{4f} - nickel feeding rate, $1/s$
R - universal gas constant, 8.3145 $J/(molK)$
r_3 - analysis accuracy of pH analyzer
r_4 - analysis accuracy of Nickel ion analyzer
T - temperature, K
T_i - integration time
t - plating time, s
t_{end} - end time of the calibration sequence, s
u_t - vector of controls used for control, $u_t = [Q_{3f}, Q_{4f}]^T$
u_1 - thermodynamic equilibrium potential of oxidation reaction, V
u_2 - thermodynamic equilibrium potential of phosphor deposition reaction, V
u_3 - thermodynamic equilibrium potential of hydrogen gas evolution reaction, V
u_4 - thermodynamic equilibrium potential of nickel deposition reaction, V
W - model-prediction error: Wiener process
x_a - thickness of the Ni-P-alloy film, cm
x_{Ni} - partial thickness of nickel, cm
x_P - partial thickness of phosphorous, cm
x^*_{Ni} - target thickness of nickel, cm
x^*_P - target thickness of phosphorous, cm
z_t - bath loading level

Greek Symbols

α_{a1} - anodic apparent transfer coefficient of oxidation reaction
α_{a2} - anodic apparent transfer coefficient of phosphorous deposition reaction
α_{a3} - anodic apparent transfer coefficient of hydrogen gas evolution reaction
α_{a4} - anodic apparent transfer coefficient of nickel deposition reaction
α_{c1} - cathodic apparent transfer coefficient of oxidation reaction
α_{c2} - cathodic apparent transfer coefficient of phosphorous deposition reaction
α_{c3} - cathodic apparent transfer coefficient of hydrogen gas evolution reaction
α_{c4} - cathodic apparent transfer coefficient of nickel deposition reaction
ε - analysis error: standard Gaussian variable
ζ - vector of optimal tracking trajectory, $\zeta = [\zeta_3, \zeta_4]^T$
ζ_3 - optimal tracking trajectory of pH
ζ_4 - optimal tracking trajectory of nickel percentage
η_1 - overpotential of oxidation reaction, V
η_2 - overpotential of phosphorous deposition reaction, V
η_3 - overpotential of hydrogen gas evolution reaction, V
η_4 - overpotential of nickel deposition reaction, V
κ^{-1} - $2k \lg e$
μ_1 - dimensionless empirical limiting coefficient of oxidation reaction
μ_2 - dimensionless empirical activating coefficient of phosphorous deposition reaction
μ_3 - dimensionless empirical limiting coefficient of hydrogen gas evolution reaction
μ_4 - dimensionless empirical activating coefficient of nickel deposition reaction
ν - robustness coefficient
ξ - vector measured pH and nickel percentage, $\xi = [\xi_3, \xi_4]^T$
ξ_3 - measured pH
ξ_4 - measured nickel percentage
ρ_{Ni} - nickel density, 8.9 g/cm^3
ρ_P - phosphorous density, 1.82 g/cm^3
σ_a - alloy deposition model inaccuracy
σ_{Ni} - nickel deposition model inaccuracy
σ_P - phosphorous deposition model inaccuracy
σ_1 - hypophosphite model inaccuracy
σ_3 - pH model inaccuracy
σ_4 - nickel ion model inaccuracy
σ_5 - sulphate model inaccuracy
σ_6 - ammonia model inaccuracy

σ_7	-	ammonium model inaccuracy
σ_8	-	orthophosphite model inaccuracy
σ_9	-	ammonium sulphate model inaccuracy
σ_{10}	-	hydrogen gas model inaccuracy
υ	-	setpoint for controls
ϕ	-	mixed potential, V
ψ	-	reaction rate coefficient, $1/s$

Abbreviations

CMI	-	Coating thickness Measurement Instrument
EDS	-	Energy Dispersive X-ray Spectrometer (a.k.a. EDX)
ENIG	-	Electroless Nickel Immersion Gold
HIE	-	Optical cross section thickness measurement
IC	-	Integrated Circuit
MEMS	-	Micro-Electro-Mechanical Systems
MTO	-	Metal Turn Over
PCB	-	Printed Circuit Board
PI	-	Proportional-Integral controller
PTH	-	Plated Thought Hole Board
PWB	-	Printed Wiring Board
SEM	-	Scanning Electron Microscope
SHE	-	Standard Hydrogen Electrode
XRF	-	X-ray fluorescence

Contents

List of Figures

Chapter 1

Introduction

1.1 Motivation

In the past decade the world has encountered the revolution of portable electronics. The electronic circuits are applied in new areas from automotive industry to portable devices like mobile phones. This development is mainly because of the success of electronic manufacturing to develop smaller, lighter and more reliable products with an increasing number of functionalities. One of the most developed manufacturing areas is the printed circuit board (PCB) manufacturing in which one sided PCBs are replaced with multilayered plated through hole (PTH) boards with dense packed integrated passive and active components. The new challenges are related not only to PCBs but also to their manufacturing processes.

A good example of such a development is mobile technology where the mobile devices, like cellular phones, contain more and more functionalities but are still small sized and reliable. The mobility poses additional requirements because the operating conditions might be moist and corrosive and the devices might be roughly handled. These set high requirements for the PCB which forms the base of the device and sets the limits for the size of the device. Because of the need for finer geometry, more dense circuitry, higher quality and better reliability of end products, there is a great interest to develop the manufacturing processes of PCBs. Especially solder joint reliability and the corrosion resistivity of PCB's surface finish are of main interest [1, 2] not forgetting the profitability and environment aspects.

In generally, PCB manufacturing process is a complex sequence of different chemical plating and etching reactions [3, 4]. A part of a manufacturing line in which one such plating reaction, electroless nickel plating, takes place is shown in Figure 1.1. As can be seen, several chemical baths, including pre and post treatments, rinsing and plating baths, are needed even during one plating process. There-

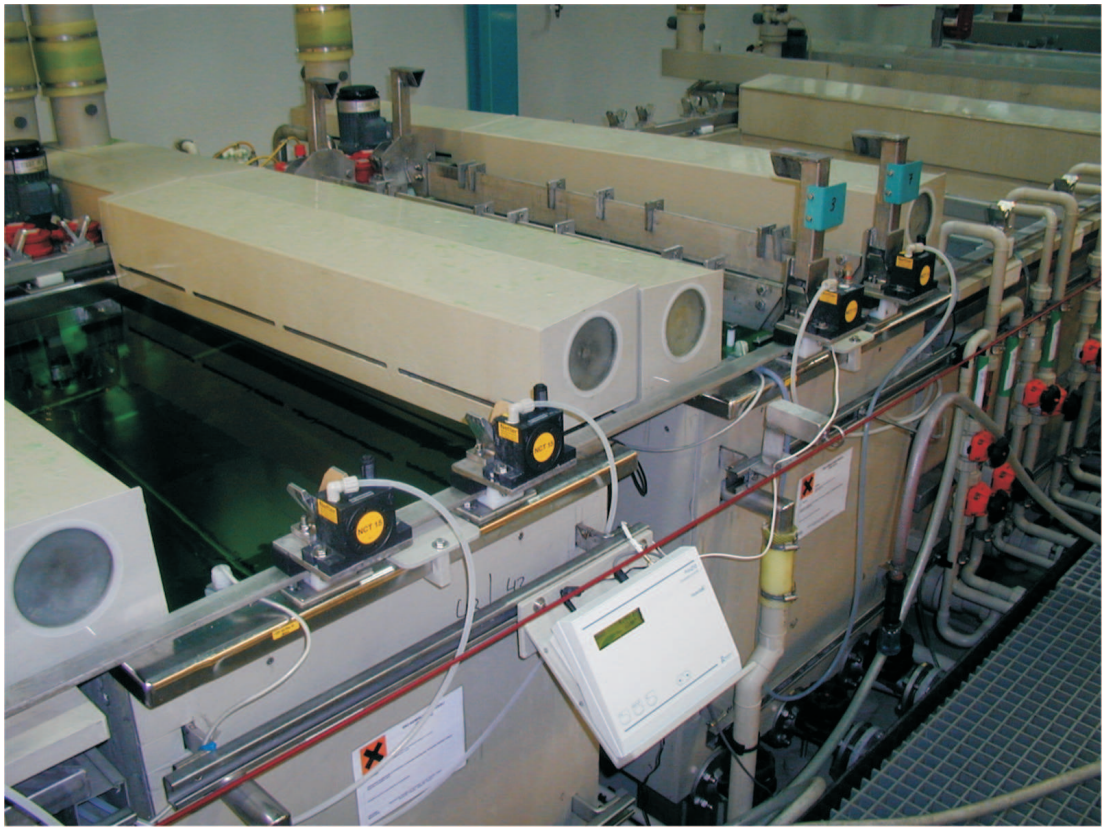

Figure 1.1: A part of electroless nickel immersion gold plating line used for PCB manufacturing.

fore, the manufacturing of multilayered PCBs needs numerous process stages and chemical processes. Because of the complexity of manufacturing and the used processes, the automation level in chemical production lines is traditionally low and the main control is manual [5, 6]. The higher production volumes, tighter product tolerances and the eagerness for better quality with lower cost has forced the producers to automate processes and to develop the process control. The benefits of this are evident, because by a precise control the plating conditions can be optimized, plating quality assured, cost of bad quality minimized and process life time extended [4]. These have further effects on the final product quality, production profitability and environmental aspects because less waste is produced. However, the development of precise process control for the plating reactions is a challenging task, because in most cases the final parameters of the plated film cannot be measured during the plating reaction. This is the case for example in electroless nickel plating which has a great effect on PCB's final properties.

1.2 Electroless Nickel Deposition

Electroless nickel plating, also known as an autocatalytic nickel plating or as a chemical nickel plating [7, 8], is a widely used plating process in many industries from oil and gas industry to microelectronic manufacturing [9]. Some of its application areas are shown in Figure 1.2. In electronic applications it is used in integrated circuit (IC) interconnections [10, 11], micro-electro-mechanical systems (MEMS) devices [12, 13] and PCBs [9, 14].

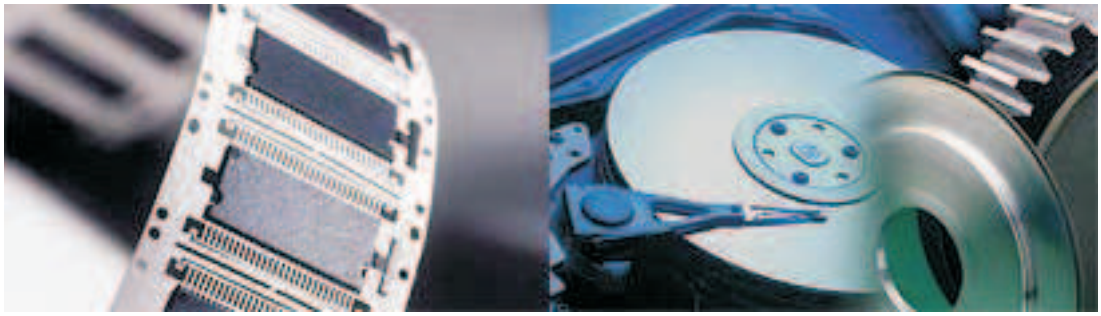

Figure 1.2: Electroless nickel plating is a widely used surface finish in many applications including electronic, hard disc and machine component manufacturing.

The progress of the electroless nickel plating reaction is depicted in Figure 1.3. In the reaction the deposited nickel is not provided by an anode but by some nickel salt. The salt is dissolved in the aqueous solution resulting ionic nickel. The nickel ions are then reduced by the electrons, not provided by an external current source but by a reducing agent also dissolved into the solution. A substrate works as a cathode and the deposition reaction occurs on its surface by a catalysis between an anodic solution and a catalytic surface, where reduced nickel catalyzes its own reduction reaction. [15]

If the original surface is not catalytically active, it has to be activated somehow to start up the autocatalytic reaction. This can be done by either connecting it to an active metal (e.g. steel), treating it with a strong reducer or it can be immersed into a dilute palladium chloride solution [9].

Electroless nickel deposit provides very good protection against corrosion [16, 17]. It has a high abrasion resistance and a good adhesion with most metals, which makes it an excellent surface finishing [7]. If compared to electroplating, electroless nickel has two major benefits: its hardness is greater and its thickness distribution is more uniform [16]. However, in electroless nickel plating the becoming deposit is not pure nickel, but contains a small amount of the reducing agent. Most commonly used reducing agent in industrial applications is hypophosphite [15] resulting in nickel phosphorous alloy [9]. The hardness, corrosion resistance

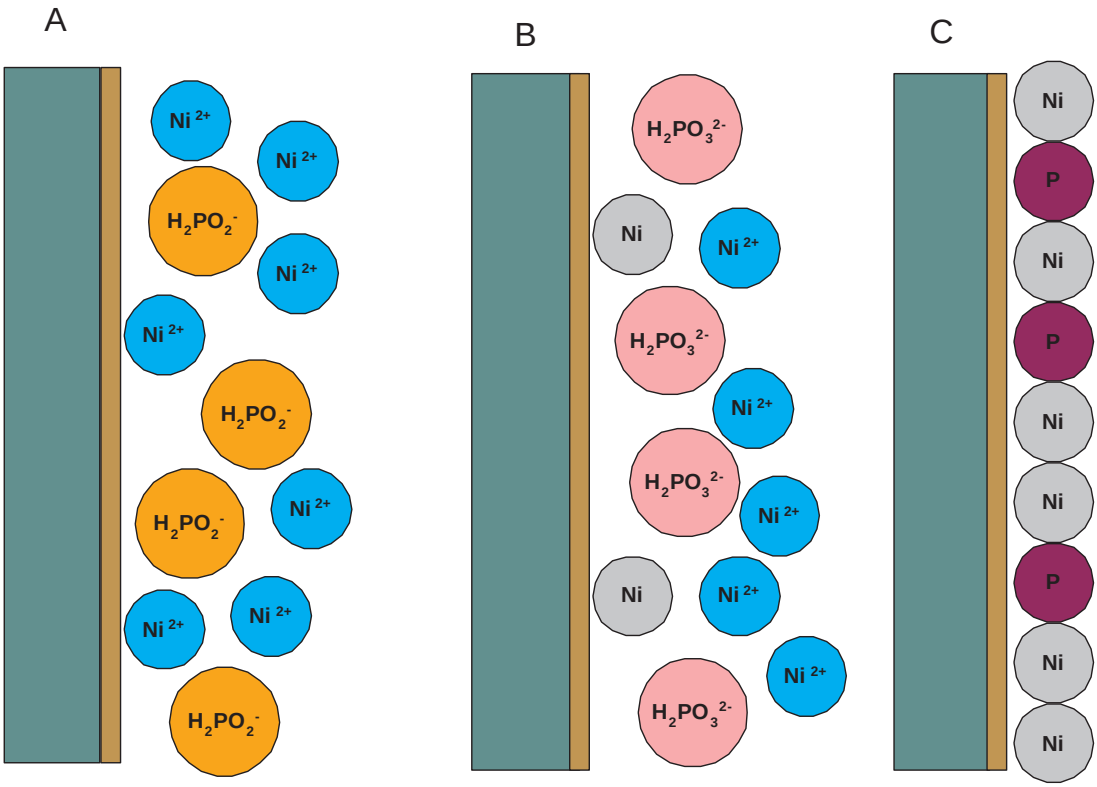

Figure 1.3: A) In electroless nickel deposition the reducing agent ($H_2PO_2^-$) and the nickel source (Ni^{2+}) are dissolved into plating bath. B) The reduction reaction occurs in an active surface where hypophosphite oxidizes into orthophosphite reducing the nickel ions into atomic nickel. C) During the reaction some reducer agent is also reduced. If the reducer is hypophosphite the plated nickel film contains some phosphorous.

and morphology of the nickel phosphorous alloy is due to the phosphorous content which can be used in the control of the alloy properties [9, 15, 18].

Although, electroless nickel is widely used and intensively studied, its reaction mechanism is not fully known, which describes the complexity of the reaction [19, 20]. It also makes the development of the process and its control challenging.

1.3 ENIG-Surface Finish

One important application of electroless nickel plating is electroless nickel immersion gold (ENIG)-surface finish used in PCB manufacturing [14, 15]. In the ENIG-surface finish, the electroless nickel alloy prevents the oxidation of a circuitry by working as a diffusion barrier between the coppered circuitry and pro-

tective gold alloy [9] as shown in Figure 1.4. In addition, it also protects the circuitry from mechanical tearing in contact surfaces [21].

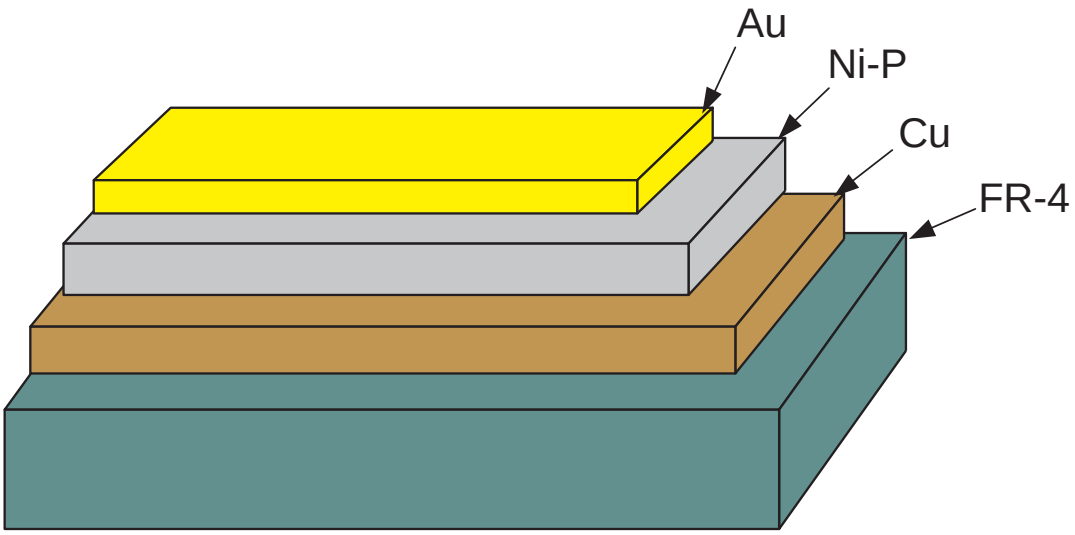

Figure 1.4: In ENIG-surface finish, electroless nickel (Ni-P) works as a diffusion barrier between copper circuitry (Cu) and golden surface layer (Au). The base material used in PCBs is typically epoxy reinforced fiberglass (FR-4)

The ENIG-process has a great effect on the PCB's final quality. Especially the thickness and phosphorous content of the electroless nickel alloy are crucial for PCB's solderability and corrosion resistance [14, 22, 23]. Unfortunately, these parameters cannot be directly measured during the plating reaction. Instead, they are measured afterwards indirectly in laboratory analysis with a delay of several hours. At that time the possible errors cannot be corrected anymore but the defective products have to be rejected. Therefore, it is crucial to control the thickness and phosphorous content of the electroless nickel alloy already during the plating process.

The ENIG-surface is lead-free, which makes it very usable for electronic applications were lead is tried to be replaced by other materials. For example in EU the use of lead in electronic products is restricted by legislation so that after 1.7. 2006 the products sold in EU markets should not contain lead more than 0.1 wt.% [24, 25, 26]. However, there is some critical problems involved in ENIG process which restrict its use. One of them is so called "black pad"-phenomenon in solder joints which is observed to be caused by many factors, one of them being the phosphorous of the electroless nickel layer [22, 27, 28]. There has been a great deal of research done around the world to understand and solve this problem. Although, it stands to reason that the "black pad" is also caused by prior and post nickel processes, the electroless nickel layer and its phosphorous content have

a great effect on the phenomenon [27, 28]. In addition, they have also an effect on other quality properties of PCB like on corrosion resistance and solderability. Therefore, the development of an effective method for the control of electroless nickel plating process is highly motivated.

1.4 Outline of the Thesis

In this thesis, a new model along with a method for the control and estimation of a electroless nickel plating process, is developed. The thesis content is the following:

Chapter 2: The developed process model for an electroless nickel reaction is introduced. The model is based on electrochemical reaction mechanisms and mixed potential reaction. The current densities of the reactions are calculated from the Buttler-Volmer equation and controlled through the empirical formulas, which accelerate or decelerate the reactions according to the concentration of the species. The equilibrium potentials of the reactions are calculated from Nernst equation and the concentration dynamics of the species in a bath is evaluated from the mass balance, based on the current densities.

Chapter 3: The proposed process model is validated against independent data gathered from an industrial plating line. The model is shown to be able to estimate the process state, critical board and bath parameters accurately from online measurable bath parameters. In addition, the electrochemical reaction mechanism is analyzed numerically based on the mathematical model.

Chapter 4: A new model-based process monitoring system for electroless nickel plating process is introduced and validated with industrial data. The system provides an accurate estimate of the process state in terms of alloy thickness, phosphorous content, electrochemical processes and bath concentrations for multiple bath with different make up concentrations.

Chapter 5: A new effective model-based process control algorithm is introduced and simulated. The algorithms is based on a calculating an optimal tracking trajectories for bath pH and nickel ion concentration. It is shown that the alloy thickness and phosphorous content can be controlled by controlling the pH and nickel ion concentration of the bath.

The author wants to note, that the reagent concentrations of the used electroless nickel plating baths are presented to the extend relevant to the scope of the thesis. This means that the main reagents and their concentrations are presented accurately. However, the additive concentrations, i.e., the concentrations of stabilizers, complexing agents and accelerators, are not presented because they are business secrets of the chemical manufacturers. In the thesis, the effect of the

additives are taken into account through the coefficients of the model parameters.

1.5 Thesis's Contribution

The main contributions of the thesis are:

1. A new model is developed for electroless nickel plating reaction based on electrochemical reaction mechanism, mixed potential theory, Buttler-Volmer equation and mass balance.
2. The reaction model covers electrical reactions and chemical reactions and takes into account the effect of reactant concentrations and the effect of bath aging through empirical coefficients.
3. It is shown that an electrochemical reaction mechanism can be used in electroless nickel plating modelling if mixed potential theory is applied.
4. The developed model is capable of estimating the unobservable processes from measurable bath parameters.
5. The developed model can be applied in different types of electroless nickel plating reactions, i.e., the low and high phosphorous reactions, because the effect of stabilizers and complex agents are modeled through empirical coefficients.
6. The developed model is validated against independent data covering metal turn over (MTO) 0-5 and it is shown that the model is able to estimate accurately the critical deposition parameters, alloy thickness and phosphorous content, from online measurable bath parameters.
7. The developed model is able to estimate accurately the concentrations of the reactants and by-products, and the unobservable electrochemical processes from the measurable bath parameters.
8. The electrochemical reaction mechanism is analyzed numerically based on mathematical model.
9. A new model-based monitoring system for electroless nickel plating process is presented providing an accurate estimate of the process state in terms of alloy thickness, phosphorous content, electrochemical processes and bath concentrations also for multiple baths with different make up concentrations.
10. It is shown that the solderability measurements are not directly related to phosphorous content but affected also by other parameters.

11. An effective algorithm for the control of the thickness and phosphorous content of electroless nickel alloy is developed based on the electrochemically balanced tracking trajectories of pH and nickel concentration of the plating bath.

12. It is shown that the alloy thickness and phosphorous content can be controlled by controlling the pH and nickel ion concentration of the bath.

13. The developed tracking control allows separate control of the film thickness and phosphorous content and keeps the process in balance avoiding spontaneous bath decompositions caused by the unbalance of reactants and canceling the disturbances affected by the bath loading.

Chapter 2

Model Development for Electroless Nickel Plating Process of Printed Circuit Board Manufacturing

2.1 Introduction

Electroless nickel plating is an important process in many microelectronic applications like in IC [10, 11], MEMS [12, 13, 29], and PCB [9, 14] manufacturing techniques. If compared to electroplating, it has many advantages but also some drawbacks. One of the drawbacks is a lack of effective process control which is mainly because of the complex reaction mechanism and a few control parameters [6]. A common way to control the process is to keep the concentrations constant and control the alloy thickness by changing the deposition time [5]. However, this is not a very effective or accurate control strategy for more demanding applications like PCB manufacturing where also the alloy's structure and content should be controlled. Therefore a new kind of control strategy is needed [30] and a model-based method is one of these.

The feasibility of model-based methods depends on the accuracy of the used model. In this chapter, a new process model for electroless nickel plating is presented. The model is based on mixed potential theory and electrochemical reaction mechanism, proposed originally by Brenner and Riddell [31, 32].

The model´s accuracy is tested against independent data gathered from an industrial plating process in Chapter 3 and applied to estimation of the process state and to process control in Chapters 4 and 5, respectively.

2.2 Modelling history

Several reaction mechanisms have been proposed to describe the plating chemistry of electroless nickel plating process [9, 33, 34, 35, 36, 37]. Despite intensive studies there exists no consensus of the right mechanism and further research is needed [19, 38]. However, it seems that the most useful reaction mechanism is the electrochemical mechanism [9, 35], especially if combined with mixed potential theory [36, 39]. There has still been no strong evidence if the theory works for electroless nickel deposition e.g. with hypophosphite [19, 39].

Despite the lack of consensus in reaction mechanism, several models of the electroless nickel reaction have been developed. Some practical modelling techniques and plating principles have been presented by Brenner [40] and Gorbunova and Polukarov [41]. White and his colleagues have modelled several electrochemical reactions using rotating disc electrode [42, 43, 44]. They managed to develop a principal model for electrodeposition of amorphous Ni-P alloys [45] but not for electroless deposition process. Kim and Sohn managed to formulate a model for steady-state electroless nickel deposition using rotating disc electrode [35]. The model was complicated and its agreement with experimental data remained unclear. Further modelling studies of the electroless process have recently been carried out by Yin *et.al.* [46] and Touhami *et.al.* [47].

Despite intensive studies no accurate and practical reaction model has been found so far [15]. This thesis presents a new model for the plating process. It is based on the same principles as the model of Kim and Sohn [35] and uses the same electrochemical cell model originally developed for porous electrodes in [48, 49].

2.3 Contribution

The following contributions are covered in this Chapter:

1. A new model is developed for electroless nickel plating reaction.
2. The electroless nickel reaction is modeled completely including electrical and chemical reactions.
3. The model is based on the electrochemical reaction mechanism, mixed potential theory, Buttler-Volmer equation and mass balances. It is shown that electrochemical reaction mechanism can be used in electroless nickel plating modelling if mixed potential theory is applied.
4. The model takes into account the empirical effect of reactant concentrations.
5. The model is capable of including the effect of bath aging.

6. The model is capable of estimating both the observable and unobservable processes from measurable bath parameters.

7. The effect of stabilizers and complex agents are modeled through coefficients and therefore the model can be applied if different additives are used.

2.4 Reactions

For hypophosphite reduced electroless nickel plating reaction four mechanisms have been proposed. These are atomic hydrogen, hydride transfer, metal hydroxide and electrochemical mechanisms [9, 20, 33, 37, 50]. Nowadays the electrochemical reaction mechanism is the most obvious [20] and because of its simplicity also the most practical one. It is used also in this thesis as a basis for the reaction model.

The electrochemical mechanism of the deposition reaction can be described through the anodic and cathodic reactions [9, 50]:

Anodic reaction

$$H_2PO_2^- + H_2O \rightleftarrows \quad H_2PO_3^- + 2H^+ + 2e^-, \qquad U_1 = -0.504V \tag{2.1}$$

Cathodic reactions

$$H_2PO_2^- + 2H^+ + e^- \rightleftarrows \quad P + 2H_2O, \qquad U_2 = -0.391V \tag{2.2}$$

$$2H^+ + 2e^- \rightleftarrows \qquad H_2, \qquad U_3 = 0V \tag{2.3}$$

$$Ni^{2+} + 2e^- \rightleftarrows \qquad Ni, \qquad U_4 = -0.257V \tag{2.4}$$

In the anodic reaction hypophosphite oxidizes to orthophosphite. In the cathodic reactions hypophosphite reduces to atomic phosphorous, hydrogen ions to hydrogen gas and nickel ions to atomic nickel. Both the atomic phosphorous and the atomic nickel depose on the substrate's surface forming nickel phosphorous (Ni-P) alloy. The potentials U_1 - U_4 are the equilibrium potentials of each of the reactions, measured at standard 25°C temperature against the standard hydrogen electrode (SHE). Therefore, they are also called as standard electrode potentials.

In the total redox reaction, the hydrogen ion production exceeds its consumption and the excess hydrogen ions decrease the bath's pH [51]. To balance the pH, a

neutralizing ammonia is added to the bath and the following neutralizing reaction takes place:

$$NH_3 + H_3O^+ \rightleftharpoons NH_4^+ + H_2O. \tag{2.5}$$

In the reaction ammonia dissolves into the bath forming ammonium and hydroxyl which neutralizes the excess hydrogen ions. The base dissociation constant of ammonia

$$Kb = \frac{[NH_4^+][OH^-]}{[NH_3]} \tag{2.6}$$

is $Kb = 1.8^{-5}$ at 25°C and at 80°C 4-5 times bigger.

The ammonium is expected to react further with sulphate forming ammonium sulphate:

$$2NH_4^+ + SO_4^{2-} = [NH_4]_2SO_4. \tag{2.7}$$

The reduction of nickel ions in aqueous solution occurs through a series of transformations and displacements. In the bulk solution, the nickel ions are surrounded by water dipoles and specific complex agents. While entering from outer Hemholtz layer into inner Hemholtz layer (absorption layer), the water dipoles and complex agents around nickel ion re-orientate allowing nickel ions migrate to the growth points on lattice metal. The reducing agent is also transferred on or close to the surface by the diffusion where it reduces the nickel ion. [46]

Although these steps play an important role in the electrochemical behavior they are not observed in rate determining [51]. It is believed in [46, 52] that a boundary layer, created by the viscosity of liquid at metal surface, may reduce the deposition speed because of lower concentration on metal surface meaning diffusion to be rate-limiting. If that would be the case, as a consequence of lower concentration, the film thickness should be proportional to the root-square of plating time according to the Fick's law

$$x = at^{1/2} \tag{2.8}$$

where
- x - film thickness, μm,
- a - constant, $a > 0$,
- t - plating time, s

as was shown in [52]. However a linear relationship

$$x = at, \tag{2.9}$$

with $a = 9.4\ \mu m/h$ was found in [51], where the film thickness $3.8 \pm 1.3\ \mu m$ was obtained at plating time $25 \pm 8\ min$ in 146 experiments, and 15 μm at plating time 90 min in 2 experiments, which matches well with linear prediction (true intercept $-0.4\ \mu m$ at zero plating time). If the diffusion would be rate-limiting, the film thickness predicted as the root-square of the plating time should be twice lower than obtained in the experiment.

Although the boundary layer may be rate-limiting in some electroless plating processes, this was not observed in the experimental data on which this dissertation is based. This might be because of the following reasons: The electric field is strong enough for dehydration in the double-layer [51]. The boundary layer on metal surface is very thin [53] because of the low viscosity at a high temperature and because of the turbulent agitation with air and recycling flows that take a place in an industrial plating line. Therefore, in this thesis, it is assumed that the deposition process is controlled by the reduction reaction instead of diffusion reaction. This rate determining reaction is represented as an electrochemical cell model in Section 2.5.

The cell model is a distributed parameter model as many other models considered in the plating literature [48, 52, 54]. Based on the cell model deposition and concentration models are developed to describe the overall process. These are represented in Sections 2.5-2.6 and compared with independent experimental data in Chapter 3.

2.5 Electrochemical cell model

The electroless nickel deposition is a redox reaction described by equations (2.1)-(2.4) with separate equilibrium potentials depending on the process circumstances. While progressing simultaneously, the potential of each of the reactions is set to one unique potential, so called mixed potential. In this potential, the overall redox reaction is in equilibrium, while the partial reactions are polarized. The difference between the mixed potential and the reaction's equilibrium potential forms the reaction's overpotential. The overpotential determines the polarity of each of the partial reactions. The hypophosphite oxidation reaction (2.1) is polarized as an anodic reaction while the rest (2.2)-(2.4) are cathodic reactions. The reaction rates can be presented through current densities calculated from Buttler-Volmer equation (2.10)-(2.13) for each of the reactions as shown in the following:

$$i_1 = i_{01}\mu_1[\exp(\nu\alpha_{a1}p_1k\eta_1) - \exp(-\nu\alpha_{c1}p_1k\eta_1)], \tag{2.10}$$

$$i_2 = i_{02}\mu_2[\exp(\nu\alpha_{a2}p_2k\eta_2) - \exp(-\nu\alpha_{c2}p_2k\eta_2)], \tag{2.11}$$

$$i_3 = i_{03}\mu_3[\exp(\nu\alpha_{a3}p_3k\eta_3) - \exp(-\nu\alpha_{c3}p_3k\eta_3)], \tag{2.12}$$

$$i_4 = i_{04}\mu_4[\exp(\nu\alpha_{a4}p_4k\eta_4) - \exp(-\nu\alpha_{c4}p_4k\eta_4)], \tag{2.13}$$

where

i_n	-	current density (n = 1, ..., 4), A/cm^2,
i_{01}	-	exchange current density, 17 $mA/cm2$,
i_{02}	-	exchange current density, 2 $mA/cm2$,
i_{03}	-	exchange current density, time-varying, $mA/cm2$,
i_{04}	-	exchange current density, 1.1 $mA/cm2$,
η_n	-	overpotential, $\eta_n = \phi - u_n$, V,
ϕ	-	mixed potential, V,
u_n	-	thermodynamic equilibrium potential, V,
μ_n	-	dimensionless concentration of species,
ν	-	robustness coefficient, 0.1,
k	-	temperature voltage, $k = F/RT$, $1/V$,
T	-	temperature, K,
R	-	universal gas constant, 8.3145 $J/(molK)$,
F	-	Faraday's constant, 96487 C/mol,
p_n	-	number of exchanged electrons, $p_1 = p_3 = p_4 = 2$, $p_2 = 1$,
α_{a1}	-	anodic apparent transfer coefficient, 0.46,
α_{a2}	-	anodic apparent transfer coefficient, 0.5,
α_{a3}	-	anodic apparent transfer coefficient, 0.56,
α_{a4}	-	anodic apparent transfer coefficient, 0.46,
α_{cn}	-	cathodic apparent transfer coefficients (n = 1-4), $\alpha_{an} = (1 - \alpha_{cn})$.

The electroless nickel bath is a multi component solution. In addition to the nickel source (nickel sulphate), the reducer (hypophosphite) and the substrate (active surface), it contains a number of additional reagents; stabilizers and complex agents, which stabilize the bath by controlling the reaction rates preventing bath contamination [9]. This effect is taken into account through the model parameters like through robustness coefficients $\nu < 1$, which make the model (2.10)-(2.13) less sensitive to the uncertainties in the equilibrium potentials.

The exchange current densities i_{0n} depend on the bath temperature T and activation energies E_{An} according to the Arrhenius equation

$$i_{0n}(T) = i_{0n}(T_0) \exp \frac{-E_{An}(T - T_0)}{RT_0T} \tag{2.14}$$

where
E_{An} - activation energy, kJ/mol,
T_0 - reference temperature, K.

Because the bath temperature in industrial plating lines is well controlled between 79 - 80°C during the plating reaction, the temperature model is not critical for current densities and a simplified model can be used [51]. An accurate approximation for the exchange current density can be obtained through the assumption that the reaction rates double for every 10 degree change in plating temperature [9]

$$i_{0i}(80\,^\circ\mathrm{C} + \Delta T) = i_{0i}(80\,^\circ\mathrm{C})[1 + \Delta T/10\,^\circ\mathrm{C}].$$

According to the mixed potential theory the anodic current density is equal to the sum of cathodic currents densities

$$i_1 + i_2 + i_3 + i_4 = 0. \tag{2.15}$$

This is because of the electrical neutrality of the plating bath. The mixed potential is a parameter adjusted by the deposition process itself to maintain the electrical neutrality; If there is any change in the partial reactions like in the concentrations or equilibrium potentials, the mixed potential assumes a value so that (2.15) is always satisfied [51].

The equilibrium potential of each the reactions (2.1)-(2.4) depends on the reagent concentrations according to the Nernst equation using unit activity for solid material (deposed nickel and phosphorous), water and hydrogen gas, as follows

$$u_1 = U_1 + \kappa(\lg c_8 - \lg c_1 - 2pH), \tag{2.16}$$

$$u_2 = U_2 + 0.2\kappa(\lg c_1 - 2pH), \tag{2.17}$$

$$u_3 = U_3 - 2\kappa pH, \tag{2.18}$$

$$u_4 = U_4 + \kappa \lg c_4, \tag{2.19}$$

where
κ^{-1} - $2k \lg e$,
c_1 - hypophosphite concentration, $molH_2PO_2^-/dm^3$,
c_4 - nickel concentration, $molNi^{2+}/cm^3$,
c_8 - orthophosphite concentration, $molH_2PO_3^-/dm^3$.

In equation (2.17) the empirical molar activity coefficient 0.2 is introduced to maintain the phosphorous deposition process cathodic. This is because of the stabilizer, used for controlling the plating reactions and preventing the spontaneous precipitation, are added into the plating bath. These stabilizers slow the plating reaction and, despite their low concentration, they have a strong influence on the reaction dynamics. Therefore, the phosphorous reactions does not follow exactly the Nernst equation and an empirical coefficient has to be introduced to calibrate the equation.

The equilibrium potentials U_n of the reactions (2.1)-(2.4) are evaluated at 25°C while the plating reaction takes place at 80°C temperature. Although, the temperature difference has a minor effect on the equilibrium potentials the difference can be taken into account by correcting the equilibrium potentials through the following temperature coefficients ($mV/°C$) [55]

$$\Delta U_1 = -0.36 \cdot 10^{-3}(T - 25\,°\mathrm{C}),$$

$$\Delta U_2 = -0.42 \cdot 10^{-3}(T - 25\,°\mathrm{C}),$$

$$\Delta U_3 = 0,$$

$$\Delta U_4 = 0.6 \cdot 10^{-4}(T - 25\,°\mathrm{C}).$$

In addition to equilibrium and mixed potentials, the current densities are also depended on concentrations through the following empirical limiting coefficients μ_1, μ_3 and activating coefficients μ_2, μ_4:

$$\mu_1 = \frac{c_1}{\lambda_1 c_1 + (1-\lambda_1)c_{1ref}}, \qquad \lambda_1 = 0.7, \tag{2.20}$$

$$\mu_2 = \left[\lambda_2 + (1-\lambda_2)\frac{c_{3ref}}{c_3}\right]\left[1 + \lambda_5 \frac{c_5}{c_{5max}}\right], \quad \lambda_2 = 0.5, \lambda_5 = 0.2, \; c_{5max} = 1.25, \tag{2.21}$$

$$\mu_3 = \frac{c_3}{\lambda_3 c_3 + (1-\lambda_3)c_{3ref}}, \qquad \lambda_3 = 0.59, \tag{2.22}$$

$$\mu_4 = \frac{c_4}{c_{4ref}} + \left[\lambda_4 + (1-\lambda_4)\frac{c_{3ref}}{c_3}\right], \qquad \lambda_4 = 0.56, \tag{2.23}$$

where

c_i	-	ion concentration of species (c_1 for hypophosphite, c_3 for hydrogen ion, c_4 for nickel, c_5 for sulphate), mol/dm^3,
c_{iref}	-	reference concentration of species (after makeup), mol/dm^3,
c_{5max}	-	maximum value of sulphate concentration, mol/dm^3.

The effect of the concentration can be seen more clearly from the coefficients (2.20)-(2.23) than from the equilibrium and mixed potentials. In coefficient (2.20), the oxidation rate is limited by a lower hypophosphite concentration, in coefficient (2.22), the hydrogen gas formation is limited by a lower hydrogen ion concentration and in coefficient (2.23), the nickel deposition rate is limited by a lower nickel concentration.

These limitations (2.20), (2.22) are weak and their effect are eliminated if $\lambda_n = 1$, but for nickel (2.23) the limitation effect is strong. The coefficients (2.21), (2.23) have the reverse effect and therefore they are regarded as activation coefficients.

The nickel deposition rate increases if the hydrogen ion concentration decreases [9]. In the model this behavior is observed through the activation coefficient (2.23) which magnifies the effect of the mixed and equilibrium potentials respectively.

The phosphorous deposition rate decreases if the hydrogen ion concentration decreases [9, 35]. In the model this behavior is seen through the activation coefficient (2.21) which reduces the effect of the mixed and equilibrium potentials respectively.

For simplicity, the previous electrochemical cell model is assumed to be deterministic and accurate, and therefore no stochastic coefficient is introduced in equations (2.10)-(2.23). The inaccuracies can be taken into account in the model outputs, i.e., in the following deposition and concentration dynamic models, because these models are linear and the possible inaccuracies in the electrochemical entries can therefore be assumed to accumulate to the inaccuracies of these models.

2.6 Plating rate

The deposition process can be decomposed into two independent processes - into nickel and phosphorous deposition - and reunited by superposition into the calculation of the nickel-phosphorous-alloy (Ni-P-alloy) film [51, 56].

Nickel deposition

According to the Faraday's law, the total deposited mass in an electrode is related to the total charge passed through it. Therefore, the nickel deposition rate is

proportional to the current density of the nickel deposition reaction (2.4)

$$dx_{Ni} = -i_4 \frac{M_{Ni}}{2F\rho_{Ni}} dt + \sigma_{Ni} dW, \tag{2.24}$$

where

x_{Ni}	-	partial thickness of nickel, cm; physically, this is a ratio between volume of nickel and plate area,
i_4	-	current density of nickel deposition reaction, A/cm^2,
M_{Ni}	-	molecular weight of nickel, 58.7 g/mol,
ρ_{Ni}	-	nickel density, 8.9 g/cm^3
σ_{Ni}	-	nickel deposition model inaccuracy,
W	-	model-prediction error: Wiener process.

Here the Wiener process is introduced to describe model's inaccuracy, i.e., it describes the error between the model estimated and the actual reaction rates. This stochastic variable is motivated especially in the Chapter 5, where developed control is simulated.

Phosphorous deposition

The deposition rate of phosphorous is, respectively, proportional to the current density of the phosphorous deposition reaction (2.2)

$$dx_P = -i_2 \frac{M_P}{F\rho_P} dt + \sigma_P dW, \tag{2.25}$$

where

x_P	-	partial thickness of phosphorous, cm; physically, this is a ratio between volume of phosphorous and plate area,
i_2	-	current density of phosphorous deposition reaction, A/cm^2,
M_P	-	molecular weight of phosphorous, 31 g/mol,
ρ_P	-	phosphorous density, 1.82 g/cm^3
σ_P	-	phosphorous deposition model inaccuracy.

Alloy deposition

The overall deposition rate of the Ni-P-alloy film is proportional to the current densities of the electrochemical reactions (2.2) and (2.4)

$$dx_a = (-i_4 \frac{M_{Ni}}{2F\rho_{Ni}} - i_2 \frac{M_P}{F\rho_P}) dt + \sigma_a dW, \tag{2.26}$$

where
x_a - thickness of the Ni-P-alloy film, $x_a = x_{Ni} + x_P$, cm
σ_a - alloy deposition model inaccuracy.

In PCB manufacturing the deposition rate is usually kept in the range of 12-15 $\mu m/h$ to guarantee the alloy quality. The thickness of Ni-P-alloy film can be calculated from the deposition rate by integrating (2.26) over the plating period (15-25 min) using the respective current densities. The partial thicknesses of the nickel or phosphorous can be calculated by integration of (2.24) or (2.25) respectively.

Phosphorous content

The phosphorous content in the Ni-P-alloy film can be expressed as the volumetric ratio between the partial and overall thicknesses

$$P_{vol} = \frac{x_P}{x_a} 100\ \% \tag{2.27}$$

or as the weight ratio between the partial and overall weights

$$P_{wt} = \frac{\rho_P x_P}{\rho_P x_P + \rho_{Ni} x_{Ni}} 100\ \%. \tag{2.28}$$

The Ni-P alloys can be classified into three categories according to its phosphorous content: low P about 1-4 wt.%, medium P about 4-11 wt.% and high P over 11 wt.% [57]. The morphology of the alloy depends on the phosphorous content: low P alloys are phosphorous supersaturated solid solutions of nickel nanocrystalline while high P alloys have amorphous structure [18]. The medium P alloys are a mixture of nanocrystalline and amorphous structures [58]. The Ni-P-alloy with 7-10 wt.% phosphorous is well solderable, corrosion resist and bondable [58] - it meets the requirements for PCB boards. However, for some products the phosphorous content should be higher [51]. In that case, the deposition rates should be slowed down to prevent surface blackening with phosphorous film. The blackening is observed to be caused by a too high hydrogen gas evolution rate [59], i.e., its current density exceeds certain threshold.

2.7 Concentration dynamics

Although, electroless nickel plating is a batch process, the batch lifespan is increased by compensating reagent consumption by feeding fresh reagents into bath. The age is measured with metal turn over (MTO). The bath's lifetime is normally

3-5 MTO, meaning that the reaction has consumed 3-5 times its initial nickel mass [51]. At that time the bath contains disruptive amount of reaction's by-products and it is discarded. These changes in the concentrations of species can be modeled through mass balances and Wiener processes as discussed below.

Hypophosphite feeding and consumption

In the studied process the reducer is hypophosphite taking part in the reactions (2.1), where it is oxidized to orthophosphite, and (2.2), where it is reduced to phosphorous. Hypophosphite source is sodium hypophosphite, added to bath during plating to compensate the hypophosphite consumption. The consumed hypophosphite mass can be calculated from the current densities i_1 and i_2 and the added mass from the measured refreshment flow rates. The concentration changing rates can be calculated by the following equation and the actual concentration c_1 by integrating the equation over bath's lifetime.

$$dc_1 = [A\frac{2i_2 - i_1}{2F} + Q_{1f}c_{1f}]dt + \sigma_1 dW, \qquad c_1(t_0) = c_{1ref}, \tag{2.29}$$

where
- c_1 - hypophosphite concentration, $mol\ H_2PO_2^-/dm^3$,
- c_{1f} - feeding solution concentration, 3.8 $mol\ H_2PO_2^-/dm^3$,
- Q_{1f} - hypophosphite dilution rate defined as the ratio between feeding rate and bath volume, $1/s$,
- A - bath loading defined as the total metal area of plates immersed in the solution per bath volume, cm^2/dm^3,
- t - elapsed time, sec,
- t_0 - makeup moment for a newly made bath, s,
- σ_1 - hypophosphite model inaccuracy.

Orthophosphite accumulation

In the reaction (2.1) hypophosphite is oxidized to passive orthophosphite. The oxidation rate is related to i_1 as follows:

$$dc_8 = A\frac{i_1}{2F}dt + \sigma_8 dW, \qquad c_8(t_0) = 0, \tag{2.30}$$

where
- c_8 - orthophosphite concentration, $mol\ H_2PO_3^-/dm^3$
- σ_8 - orthophosphite model inaccuracy.

Nickel ion feeding and consumption

In the studied process the nickel source is nickel sulphate ($NiSO_4$) which dissolves in aqueous solutions into Ni^{2+} and SO_4^{2-} ions. The nickel ion takes part in reaction (2.4) where it is reduced to metallic nickel by the electrons donated by hypophosphite. The consumed nickel is replaced by nickel sulphate pumping. The model of nickel ion concentration follows the same principle as hypophosphite model and is presented below

$$dc_4 = [A\frac{i_4}{2F} + Q_{4f}c_{4f}]dt + \sigma_4 dW, \qquad c_4(t_0) = c_{4ref}, \tag{2.31}$$

where

c_4	-	nickel concentration, $mol\ Ni^{2+}/dm^3$,
c_{4f}	-	feeding concentration, 1.8 $molNi^{2+}/dm^3$,
Q_{4f}	-	nickel dilution rate, $1/s$
σ_4	-	nickel ion model inaccuracy.

Hydrogen ion formation and removal with ammonia

During the electroless deposition reaction (2.1)-(2.4) the hydrogen ion production exceeds its consumption. Because of the formed hydrogen the pH decreases, which is balanced by ammonia additions. The neutralization reaction is

$$NH_3 + H_3O^+ \rightleftharpoons NH_4^+ + H_2O \tag{2.32}$$

where

$$K_a = \frac{[NH_3][H^+]}{[NH_4^+]} = \frac{k_f}{k_b}, \tag{2.33}$$

K_a	-	acid dissociation constant for ammonia, $K_a = K_w/K_b$,
K_w	-	water dissociation constant, $K_w = 10^{-14}$ at 25 °C,
k_f	-	advancing reaction rate, $k_f = 1.5 \cdot 10^{-4}\ mol\ NH_3/s$,
k_b	-	inverse reaction rate, $k_b = 1.8 \cdot 10^5\ mol\ NH_4^+/s$.

If the balance of (2.32) is disturbed, the system finds a new equilibrium that reserves the ratio (2.33) by changing the concentration of the reagents, respectively. The change dx is called equilibrium increment and its value is equal in all the reagents:

$$dx = dx_3 = dx_6 = dx_7, \tag{2.34}$$

where
dx - equilibrium increment, $mol\ H^+/dm^3$,
dx_3 - dissociation consumed hydrogen ions, $mol\ H^+/dm^3$,
dx_6 - dissociation consumed ammonia, $mol\ H^+/dm^3$,
dx_7 - dissociation produced ammonium, $mol\ H^+/dm^3$.

If the reaction occurs in an acidic solution, as is the case in hypophosphite reduced reaction, practically all the ammonia is consumed by the neutralization reaction and the balance of reaction (2.32) is completely on the product side. Therefore, the equilibrium increment is directly the added ammonia concentration:

$$\frac{dx}{dt} = Q_{3f}c_{3f}. \tag{2.35}$$

where
c_{3f} - feeding concentration, 0.4 $mol\ NH_3/dm^3$,
Q_{3f} - ammonia dilution rate, $1/s$,

In plating reaction the hydrogen ion production rate is related to i_1 and its consumption to i_2 and i_3. By ammonia addition the excess hydrogen ions is neutralized by the amount of dx_3. Therefore the hydrogen ion concentration can be modeled through mass balance as

$$dc_3 = A\frac{i_1 + 2i_2 + i_3}{F}dt - dx_3 + \sigma_3 dW, \qquad c_3(s_0) = c_{3ref}, \tag{2.36}$$

where
c_3 - hydrogen ion concentration, $mol\ H^+/dm^3$
σ_3 - pH model inaccuracy.

The concentration of the added ammonia can be modeled calculating the difference of added and dissolved concentrations as follows

$$dc_6 = Q_{3f}c_{3f}dt - dx_6 + \sigma_6 dW, \qquad c_6(t_0) = 0, \tag{2.37}$$

where
c_6 - ammonia concentration, $mol\ NH_3/dm^3$
σ_6 - ammonia model inaccuracy.

If the acidic plating bath is assumed, all the ammonia is consumed by the neutralization reaction and therefore $dc_6 = 0$.

Ammonium, sulphate and ammonium sulphate formation and consumption

As a consequence of the neutralization reaction, ammonium is formed in the bath. This ion is active and, if formed excessively, it can react with sulphate ions SO_4^{2-} forming ammonium sulphate as shown below

$$2NH_4^+ + SO_4^{2-} \rightarrow [NH_4]_2SO_4 \tag{2.38}$$

The formation of solid ammonium sulphate is unlikely because ammonium sulphate is highly soluble into aqueous solutions (760 g/dm^3 H_2O at 20 °C). However, if the ammonium sulphate precipitation is observed, it deposits sediments to the bottom of the bath. The formation rate is proportional to the concentrations of sulphate and ammonium, and the concentrations of the sulphate, ammonium and ammonium sulphate can be modeled through mass balance as follows

Sulphate:

$$dc_5 = [Q_{4f}c_{4f} - \psi c_5 c_7]dt + \sigma_5 dW, \qquad c_5(t_0) = 0, \tag{2.39}$$

where
- c_5 - sulphate concentration, $mol\ SO_4^{2-}/dm^3$,
- c_7 - ammonium concentration, $mol\ NH_4^+/dm^3$,
- c_{4f} - sulphate feeding concentration, equal to the nickel feeding concentration, 1.8 $mol\ SO_4^{2-}/dm^3$,
- Q_{4f} - sulphate dilution rate, equal to the nickel dilution rate, $1/s$,
- ψ - reaction rate coefficient, $1/s$
- σ_5 - sulphate model inaccuracy.

Ammonium:

$$dc_7 = dx_7 - 2\psi c_5 c_7 dt + \sigma_7 dW, \qquad c_7(t_0) = 0, \tag{2.40}$$

where
- σ_7 - ammonium model inaccuracy

Ammonium sulphate:

$$dc_9 = \psi c_5 c_7 dt + \sigma_9 dW, \tag{2.41}$$

where
- c_9 - ammonium sulphate concentration, $mol\ [NH_4]_2SO_4/dm^3$
- σ_9 - ammonium sulphate model inaccuracy.

If the precipitation is not observed, its effect can be canceled from the equations (2.39)-(2.41) by setting $\psi = 0$. The possible ammonium sulphate precipitate is mainly passive but along with other solid by-products and impurities, it interferes the electroless deposition reaction and might cause sudden bath contamination. This can be avoided by effective filtering or changing the bath when MTO reaches 3-5.

Hydrogen gas evolution

The hydrogen gas formed in reaction (2.2) is related to i_2. The gas evaporates from the bath and does not disturb the reaction. The concentration of the gas formed into the bath can be modelled as the following if the evaporation is not taken into account

$$dc_{10} = -A\frac{i_3}{2F}dt + \sigma_{10}dW, \tag{2.42}$$

where
dc_{10}/dt - hydrogen gas evolution rate, $mol\ H_2(g)/(sdm^3)$
σ_{10} - hydrogen gas model inaccuracy.

In general, the plating chemistry is rather complex and still incompletely understood [9, 33] especially with respect to hydrogen ion. Its formation, utilization and evolution to gas are more complex than shown in the reactions (2.1)-(2.3), (2.32) as well as the influence of stabilizers, orthophosphite, ammonium sulphate, MTO variation and other by-products. The Wiener processes are introduced in models (2.37)-(2.36), (2.30)-(2.42) because of modelling inaccuracies which should be accounted for in the development of the estimation and control strategy, discussed in the following Chapters.

2.8 Conclusions

In this Chapter, a novel model for electroless nickel plating is presented. The model is based on the electrochemical reaction mechanism and mixed potential theory. In addition, the Buttler-Volmer equation, Nernst equations and mass balance are used for the modelling of current densities, equilibrium potentials and concentration dynamics, respectively.

The model is developed primarily for the ENIG process of PCB manufacturing industry and therefore, its input consists of the online measurable parameters, used commonly in the industry. These are the reagent concentrations and the amounts of the added reagents, plating temperature, bath loading and plating time. The model is capable of estimating the complete electroless nickel plating

reaction including electrical and chemical reactions. It takes into account both the theoretical electrochemical principles and the empirical effects of reactant concentrations, including the effect of bath aging.

The model can be used for estimating the critical deposition processes and the unobservable electrochemical processes of the electroless nickel plating reaction. It contains parameters that are calibrated from the experimental data gathered from an industrial plating process. The physical equivalence of these are the additive concentrations, like stabilizer, complex agent or accelerator concentrations, which have the same kind of effect to the real reaction as the parameters have to the model behavior. By changing calibration, the model can be applied for different types of electroless nickel baths with different additive concentrations.

Generally, the developed model is a promising tool for monitoring the unobservable processes in PCB industry. Its accuracy is validated using independent data in Chapter 3 and its application to process monitoring and control are presented in Chapters 4 and 5.

Chapter 3

Model Validation and Process Analysis

3.1 Introduction

The model, introduced in Chapter 2, is validated against process data gathered from an industrial PCB manufacturing line, in this Chapter. In PCB manufacturing, electroless nickel plating is used as a part of ENIG-surface finish as discussed before. For the model parametrization and validation several active and passive experiments were carried out in the line with different MTOs. In addition to normal online process measurements, some additional parameters were measured in laboratory afterwards.

The recorded data are discussed in Section 3.3 and the validation experiments in Section 3.4. Similar results observed in other experiments are discussed in [51, 56, 60, 61].

3.2 Contribution

The following contributions are covered in this Chapter:

1. The proposed model is validated against independent data covering the whole MTO range (0-5) and shown to be relatively accurate.

2. The model is capable of estimating the critical deposition parameters, alloy thickness and phosphorous content accurately from online measurable bath parameters.

3. In addition to the deposition parameters the model is capable of estimating the concentrations of the reactants and by-products.

4. Using the model it is possible to estimate the unobservable electrochemical processes from the measured data.

5. The electrochemical reaction mechanism is analyzed numerically based on the mathematical model.

6. It is shown that the electroless nickel plating reactions can be modeled using the mixed potential theory and the electrochemical reaction mechanism.

3.3 Recorded data

The data for parameter estimation and model validation were recorded during one week of active experiments and several weeks of passive experiments in the industrial plating line. In the active experiments, some plating parameters were changed according to the test schedule. Because the experiments were carried out during normal production, the changes had to be inside production tolerances. A part of the active experiment sequence is shown in Figures 3.1-3.4. In the passive experiments the data were recorded along with normal production and from many batches. During the experiment the MTO changed from 0 to 5, after which the bath was discarded. Therefore, the whole bath's life span with several loading profiles and makeups were studied and the validation was extensive.

The measurements were gathered from industrial process control databases and from process laboratory analysis. The alloy's final characteristics were measured afterwards using methods not used in normal production. Description of the measurements is presented in more details in the following.

On-line measurements

The following measurements were measured on-line and recorded every 5 seconds:

1. Nickel ion concentration presented as nickel percentage where 100 % = 0.1 $mol\ Ni^{2+}/dm^3$, (c_4)

2. pH, ($-\lg c_3$)

3. Nickel, hypophosphite and ammonia feeding rates, (Q_{4f}, Q_{1f} and Q_{3f}, respectively)

4. Plating temperature, (T)

5. Bath loading, (A)
6. Plating time, (t)
7. Mixed potential versus standard hydrogen electrode (SHE), (ϕ)

These on-line measurements are used as inputs for the developed model, which estimates other needed bath parameters and predicts the becoming alloy properties. The chemical measurements like nickel percentage and pH measurement might however involve uncertainties, which have to be also considered in the prediction results. For this purpose the mathematical models of these analyzers are presented in below.

pH analyzer

$$\xi_3 = -\lg c_3 + r_3\varepsilon = pH + r_3\varepsilon, \tag{3.1}$$

where
ξ_3 - measured pH,
c_3 - hydrogen ion concentration, $mol\ H^+/dm^3$,
r_3 - analysis accuracy
ε - analysis error: Independent Gaussian standard deviation, N(0,1).

Nickel analyzer

$$\xi_4 = 100\frac{c_4 + r_4\varepsilon}{0.1} = 10^3(c_4 + r_4\varepsilon), \tag{3.2}$$

where
ξ_4 - measured nickel percentage: 100 % is equal to 0.1 $mol\ Ni^{2+}/dm^3$,
c_4 - nickel concentration, $mol\ Ni^{2+}/dm^3$,
r_4 - analysis accuracy.

Both the nickel and pH analyzers are calibrated against reference solution once per hour. In addition these values are also measured in the laboratory. The other on-line measurements are measured with more reliable methods and thus they are considered as exact values.

Laboratory analysis

Beside online measurements, the following parameters were analyzed in the laboratory.

1. Hypo- and orthophosphite concentration

2. Thickness of plating film measured using X-ray fluorescence analyzer (XRF) a.k.a. coating thickness measurement instrument (CMI)
3. Phosphorous content measured using energy dispersive X-ray spectrometer (EDS) applied in scanning electron microscope (SEM).

These analyses take place every 5 hours. Because of the low frequency, these measurements can not be used as inputs for the developed model. The hypophosphite concentration is however an important variable for the model and therefore the model estimates hypo- and orthophosphite concentrations according to equations (2.29) and (2.30). The laboratory analyses were mainly used for model validation.

Alloy properties

The most critical alloy properties are alloy thickness and its phosphorous content [4, 60]. To measure these properties, a small test plate was plated within every production lot and the properties were measured afterwards from the plate.

The thickness was measured using an X-ray fluorescence analyzer (XRF). Each test plate was measured six times and the used thickness is the arithmetic mean of these measurements.

The phosphorous content in weight percentage was analyzed using energy dispersive X-ray spectrometer (EDS) applied in scanning electron microscope (SEM). Because phosphorous is not evenly distributed over the alloy [9, 62], 10 analyses were made over the plating area and its cross section. The used value is an arithmetic mean of these. EDS-analyses were taken after every 3 hours.

3.4 Model validation

Three active and several passive experiments were performed in the line. The recorded active data were divided into estimation and validation data to be used for parameter estimation and model validation, respectively. The passive data were gathered in normal process conditions and used only for model validation. In the following one active experiment used for model validation is discussed. Additional results from the other experiments are similar and summarized in Tables 3.2 and 3.3.

Validation sequence

The bath characteristics during the validation sequence are shown in Figures 3.1 - 3.4. During the experiment, bath loading was changed between three levels

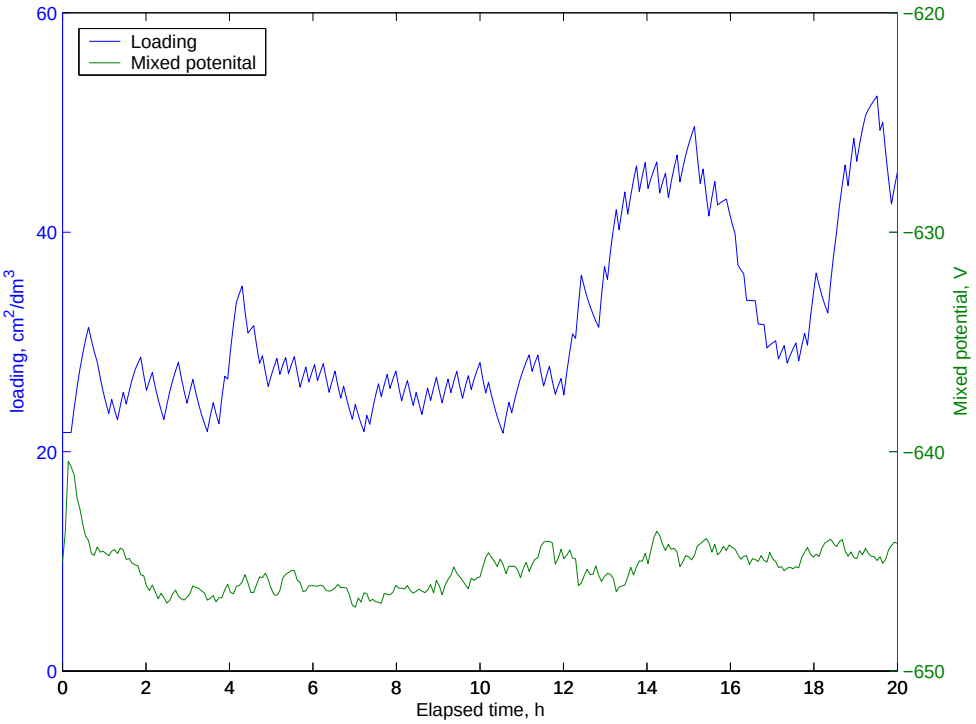

Figure 3.1: The bath characteristics during the model validation test: bath loading and mixed potential.

(20, 40 and 60 cm^2/dm^3). The bath loading is a violent jumping process where a rack of plates is immersed and raised approximately every 20 minutes. The loading shown in Figure 3.1 is a two hour moving average of the original bath loading. This is because of better visualization and comparability with the other parameters. However, the calculations are based on the original loading.

The mixed potential of the plating reaction was measured by immersing a copper plate into the bath and measuring the voltage between the plate and standard hydrogen electron. The measured mixed potential is shown in the same figure. In theory, the mixed potential depends on concentrations, bath loading and plating temperature. This is, however, hard to see from the figure because all of these are changed during the experiment and not returned to their original values. Still, correlation can be observed especially with loading, temperature, nickel concentrations and pH.

The reference value of the nickel ion Ni^{2+} concentration in the used plating chemistry is 0.1 mol/dm^3. During the experiment, the nickel ion concentration was changed between three levels: 95, 100 and 105 % of its reference, which is equal to 0.095, 0.1 and 0.15 mol/dm^3, respectively. The nickel concentration percentage along with nickel sulphate $NiSO_4$ pumping is shown in Figure 3.2.

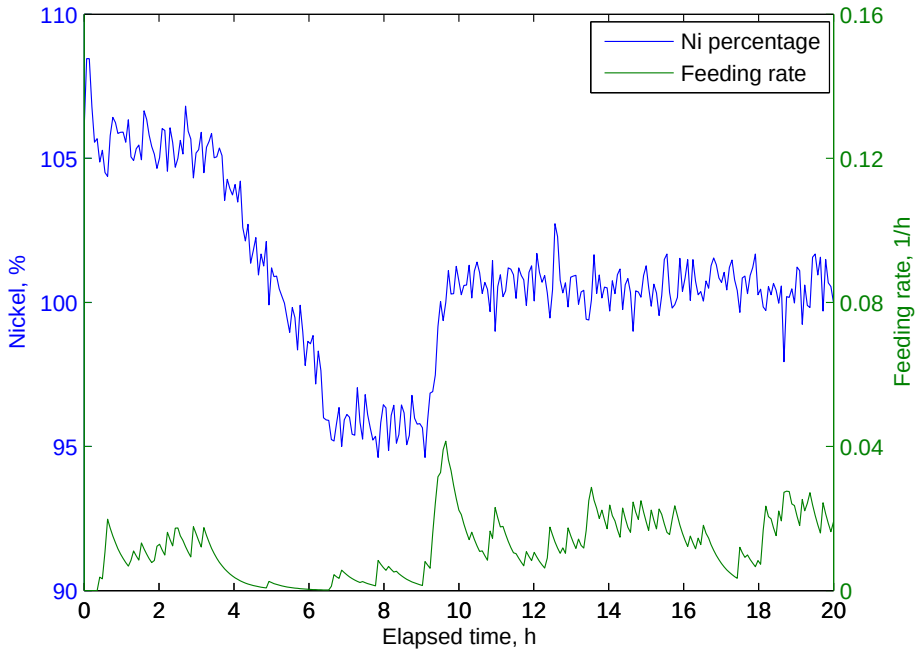

Figure 3.2: The bath characteristics during the model validation test: NI^{2+} content and $NiSO_4$ feeding rate.

The difference of the concentration time constants can easily be seen from the figure; the nickel concentration can be rapidly raised by the nickel sulphate pumping but lowering takes time and is dependent on loading. It can also be seen that the higher the loading, the higher the nickel ion consumption, which is to be expected. This can clearly be seen especially in the end of the experiment where higher pumping is needed to keep the concentration stable if the loading is high.

The same kind of effect can also be seen from the pH graph shown in Figure 3.3. During the experiment pH was controlled by ammonia pumping and changed between 5.05-5.15 as shown. Also here the pH raise is quicker than lowering. Compared to nickel ion concentration lowering the pH is slower. In this comparison the difference of loading level has to be taken into account.

The plating temperature and the plating time were kept as constant as possible during plating, because of the limits of the used chemistry and the ongoing PCB production on the line. The too low bath temperature might have stopped the reaction and too high might have resulted the bath contamination [9]. As can seen from Figure 3.4, the temperature is constant staying between 79 to 80°C during the experiment. The minor changes are due to loading events where the warm plates are replaced by those of room temperature.

Also the plating time had to be extended while MTO was raised as shown in

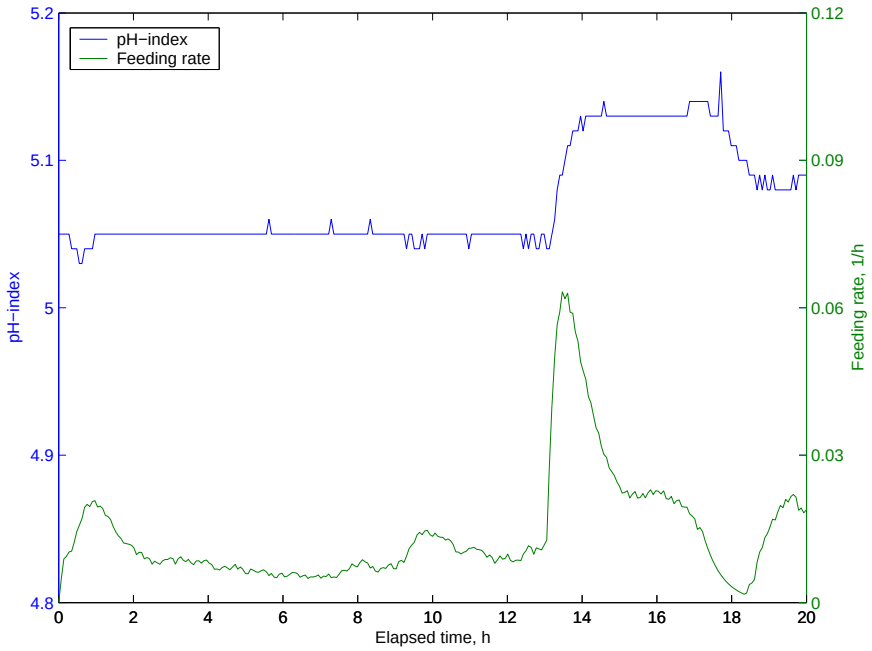

Figure 3.3: The bath characteristics during the model validation test: pH and NH_3 feeding rate

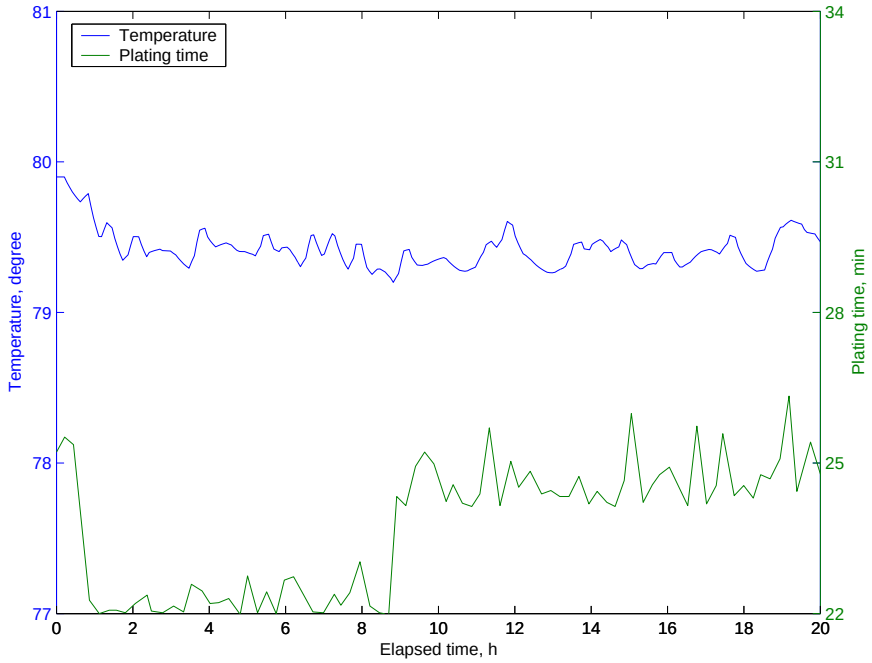

Figure 3.4: The bath characteristics during the model validation test: temperature and plating time

Figure 3.4. This is because the plating rate decreases along bath aging and because the plating time is linearly proportional to the alloy thickness, as discussed in Chapter 2.4. Therefore, the longer plating time was used to compensate the slower reaction in the end of the experiment. The long plating time in the beginning of the experiment is due to plating startup. In the startup the concentrations, the temperature and the other bath parameters are tuned to appropriate levels to ensure alloy quality. The unbalance of the parameters in the startup can also be seen from the mixed potential curve.

Table 3.1: The measurements used as inputs for the model in different partial model validations. The data numbers refer to the numbers of online measurements in Chapter 3.3.

Task	Data Compared	Data Used
Comparison of the model predicted and XRF/EDS measured thickness and phosphorous	Film thickness, Phosphorous percentage	1-7
Prediction of the nickel in comparison with the online measured nickel	Nickel concentration	2-7
Prediction of the pH in comparison with the online measured pH	pH	1, 3-7
Prediction of the hypo- and ortho-phosphate concentrations in comparison with the laboratory analysis	Hypophosphite Orthophosphite	1-7
Prediction of the nickel in comparison with the online measured nickel in passive experiments	Nickel concentration	2,3
Prediction of the pH in comparison with the measured pH in passive experiments	pH	1,3
Prediction of the board and bath parameters	Respective laboratory analysis	1-7

The model accuracy is evaluated based on these data. The estimated parameters and the data used is shown in Table 3.1. The process state is evaluated from the model using the online measurements 1-7 explained in Section 3.3. The model accuracy is analyzed by comparing the estimated state to the laboratory analysis as discussed in the following.

Deposition model validation

While considering the PCB manufacturing, the most critical values of the nickel alloy are its thickness and phosphorous content. Although, these values cannot be measured online during the plating, the developed model can estimate these values from the standard online process measurements, i.e., Ni^{2+} concentration, pH, plating time and temperature, as discussed in Chapter 2.6.

The accuracy of the deposition model is evaluated by comparing the measured alloy thickness and phosphorous content to those computed from the model as presented in Figures 3.5 and 3.6. The accuracy is also calculated numerically as a standard deviation of the measured and predicted values and then represented in normalized units as a percentage from the admissible technology range. These accuracies are presented in Table 3.2.

Table 3.2: Numerical accuracies of alloy thickness and phosphorous content (wt. %) models [60].

Parameter	Admissible range	Accuracy %	
		Estimation data	Evaluation data
MTO	0-5	0-2	3-5
Alloy thickness	2.5-5 μm	9	9
Phosphorous	7-10 wt. %	18	10

In Figure 3.5 the estimated alloy thickness curve has the same shape as the measured one. This implies that the relations between the bath conditions and deposition rates are correct and that the structure of the model is correct. The absolute values, however, differ from each other, especially in the beginning of the experiment. The reason for that is the high nickel ion concentration in the beginning, which makes the empirical activation coefficient (2.23) too high. This inaccuracy can, however, be corrected by increasing the value of c_{4ref} in the equation (2.23). Therefore, it can be stated that, although the model is accurate in general, it lacks of accuracy in high nickel ion concentrations if this parametrization is applied. The error is still relatively small if compared to the admissible range and, in practice, during normal production the nickel concentration is not that high, which improves the accuracy of the estimate. Also, if the model is supposed to be used in high nickel concentrations, it can be re-calibrated respectively. The peaks in the curve are due to peaks in the deposition time shown in Figure 3.4.

Although, the alloy thickness estimate is accurate, the phosphorous content estimate lacks of accuracy especially in the beginning of the experiment as can be seen from Figure 3.6. In general, the form of the estimated graph is close to the

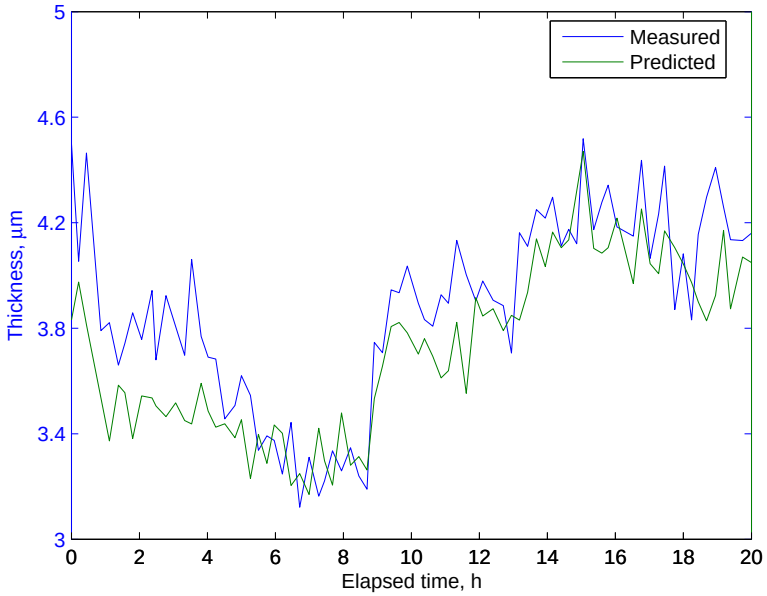

Figure 3.5: Measured and model predicted alloy thicknesses during model validation test.

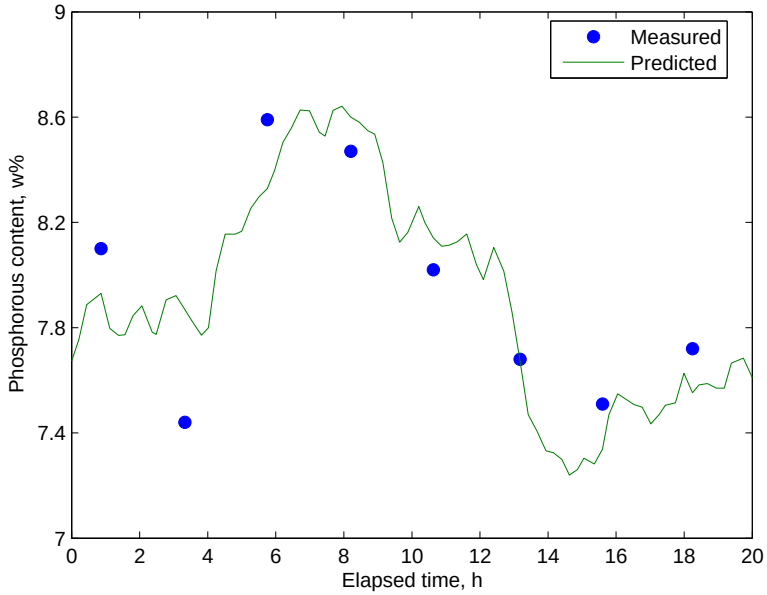

Figure 3.6: Measured and model predicted phosphorous contents of the alloy during model validation test.

measured one, but the two first measurements on the opposite sides of the estimated graph indicate that the proposed phosphorous deposition model misses some relations. However, the same data set was analyzed by using multivariable regression methods in [63] and no explanation was found for this inaccuracy. Therefore, it is likely, that this disagreement between the estimated and measured phosphorous contents is because of an exception from normal in the preceding processes, like in the activation of the surface.

In practice it has been observed that high loading corresponds to low phosphorous content. One theory to explain this phenomenon is the relation of the bath loading and the hypophosphite. If the loading is low, the hypophosphite concentration on the substrate's surface is high and multiple hypophosphite ions are reduced to phosphorous and further co-deposited. If the loading is higher the concentration is lower and less hypophosphite is reduced. The other parameter that has been observed to affect the phosphorous content in practice is pH. The relations between plating and product parameters are complicated and not fully understood [9]. These are explained in more details using the model in Section 3.5.

Despite weaknesses in the phosphorous model, the absolute estimation error is still reasonable if compared to the admissible range shown in Table 3.2.

Validation of the concentration dynamics model

Besides deposition prediction, the model can be used for reactant's concentration estimation as presented in Section 2.7. One critical concentration is the hypophosphite concentration which is estimated according to equation (2.29) and used in the nickel deposition model (2.24). It is not measured online during normal process control and therefore, accurate hypophosphite concentration estimation is crucial for whole the deposition model.

Other important concentrations are orthophosphite, nickel ion and hydrogen ion concentrations which can be calculated according to equations (2.30), (2.31) and (2.36), respectively. Although, the nickel ion concentration and pH can be measured and adjusted accurately by the process control system, the model estimated values can be used for model validation.

The model estimated and laboratory measured hypo- and orthophosphite are presented in Figure 3.7 and the numerical accuracies in Table 3.3. As can be seen from the figure, the shapes of the estimated and measured curves are the same. This implies that the basic model structures in (2.29) and (2.30) are correct.

However, there is a significant absolute error especially between the measured and estimated orthophosphite concentrations. This can be partly explained by the low sampling frequency of the laboratory analysis (ones per every 5 hour).

In practice, the orthophosphite estimate has only a minor effect on the anodic reaction's equilibrium potential (2.16) as discussed in Section 3.5 and therefore its inaccuracy is not critical to the deposition model.

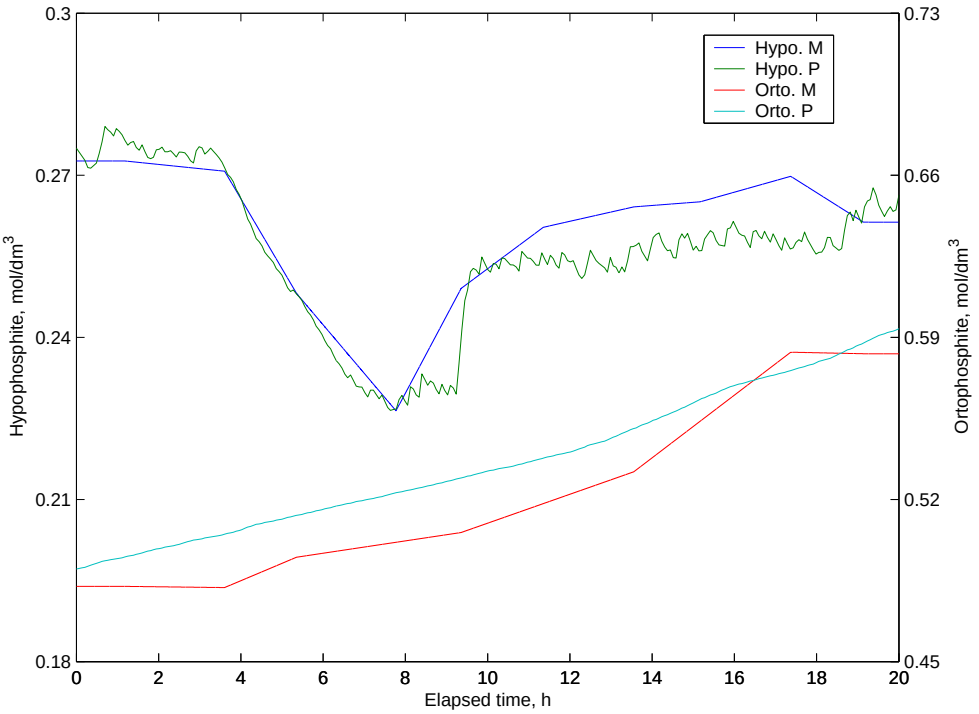

Figure 3.7: Measured (M) and model predicted (P) hypo- and orthophosphite concentrations during model validation test.

Estimated and online measured nickel concentration is presented in Figures 3.8, and the numerical accuracies in Table 3.3. The nickel model (2.31) follows the measured values accurately while the estimation error stays below 7 % of the admissible range (90-105 %). This refers to a correct model structure and model parameters. Because the model is based on a mass balance equation, where nickel is consumed according to the deposition model (2.24) and added by the refreshing pumping, it gives a strong indication that the proposed nickel deposition model is accurate.

The pH model (2.32)-(2.36) validation is presented in Figure 3.9. The estimated value follows the measured values accurately, although the rise in pH disturbs the pH model balance in the end of the experiment. This is because of the diminished capability of the buffer liquid, which make the behavior of pH more nonlinear than to which the model (2.32)-(2.36) is calibrated. Despite that the estimation error stays below 5 % of the admissible range (4.2-5.3) as shown in Table 3.3. In general, pH modelling is a challenging problem [64] and therefore the accuracy of the proposed model is good considering its simplicity. In practice, pH is an online measurable parameter and in the calculations the online measured value

Table 3.3: Numerical accuracies of pH, nickel ion (Ni^{2+}) and hypophosphite concentration models [60].

Parameter	Admissible range	Accuracy %	
		Estimation data	Evaluation data
MTO	0-5	0-2	3-5
Nickel	90-105 %	9	7
Hypophosphite	22-45 g/dm^3	7	14
pH	4.2-5.3	3	5

can be used. Therefore, the pH model inaccuracy is not critical for the deposition model.

The model accuracies of the concentration dynamics are evaluated experimentally and summarized in Table 3.3, where the accuracies are divided to the model calibration data and to independent validation data. The numerical accuracies are calculated as a standard deviation of the predicted and measured values in normalized units as a percentage from the admissible technology range. The experiments are slightly different in the metal turn over MTO, which is observed to effect positively on the alloy's phosphorous content. The MTO can be estimated from the orthophosphite accommodation and therefore the effect is taken into account in (2.21), where the activity is increased along with the orthophosphite accumulation.

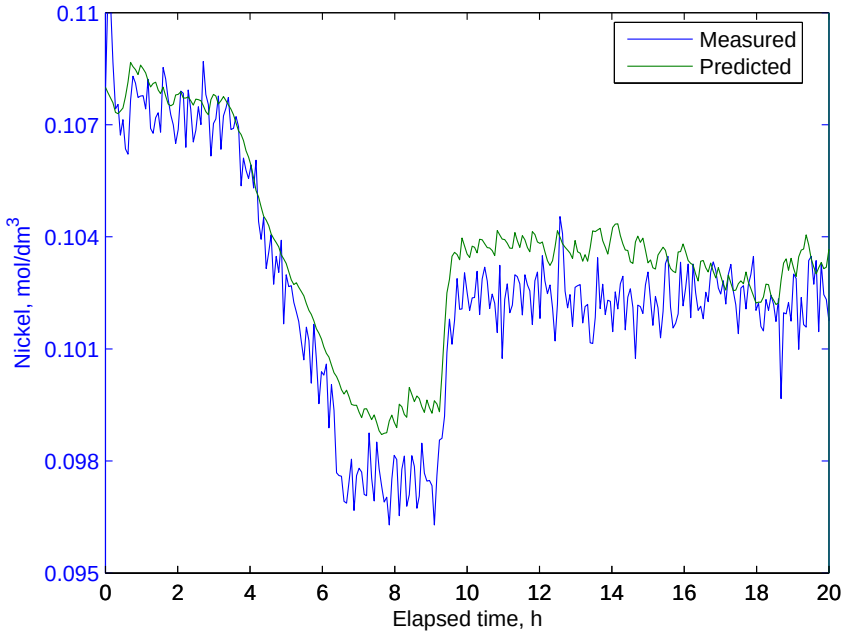

Figure 3.8: Measured and model predicted nickel ion (Ni^{2+}) concentration during model validation test

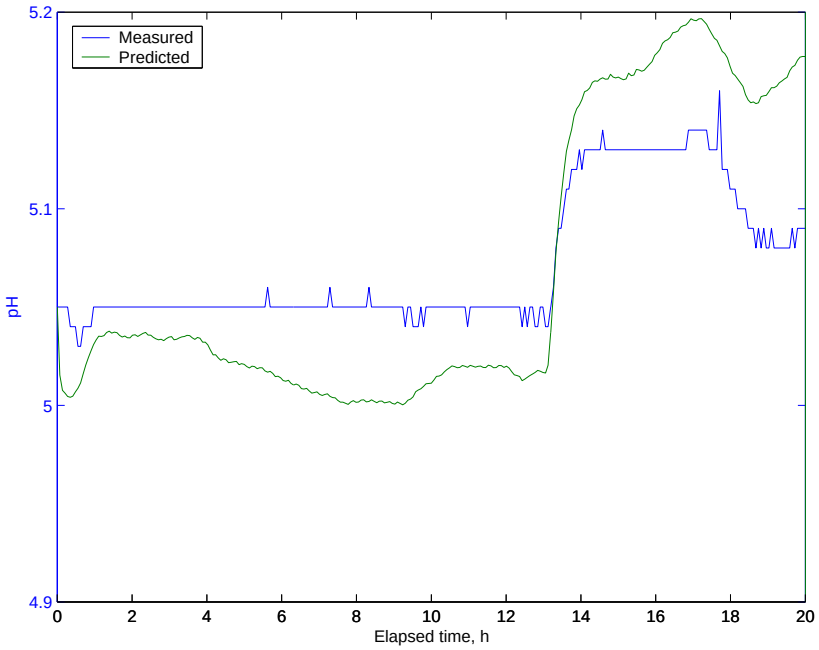

Figure 3.9: Measured and model predicted pH during model validation test

3.5 Plating reaction analysis

The electrochemical model forms the core of the plating process model and therefore it has to be accurate and well balanced to guarantee the accuracy of the overall model. The accuracy of the model cannot be directly validated because no measurements are available of the electrochemical parameters. However, the electrochemical model can be assumed to be precise if the other models derived from the electrochemical model are accurate as is the case in this research. In addition, the current densities of nickel and phosphorous deposition reactions along with the respective deposition rates can be validated indirectly by the reference values derived from the film thickness, phosphorous weight percentage and plating time measurements as shown in Figures 3.10 and 3.11. As can be seen the current density and reaction rate estimates are close to the calculated real values confirming the model validity. For further analysis all the current densities are shown in Figure 3.12 and respective equilibrium potentials in Figure 3.13.

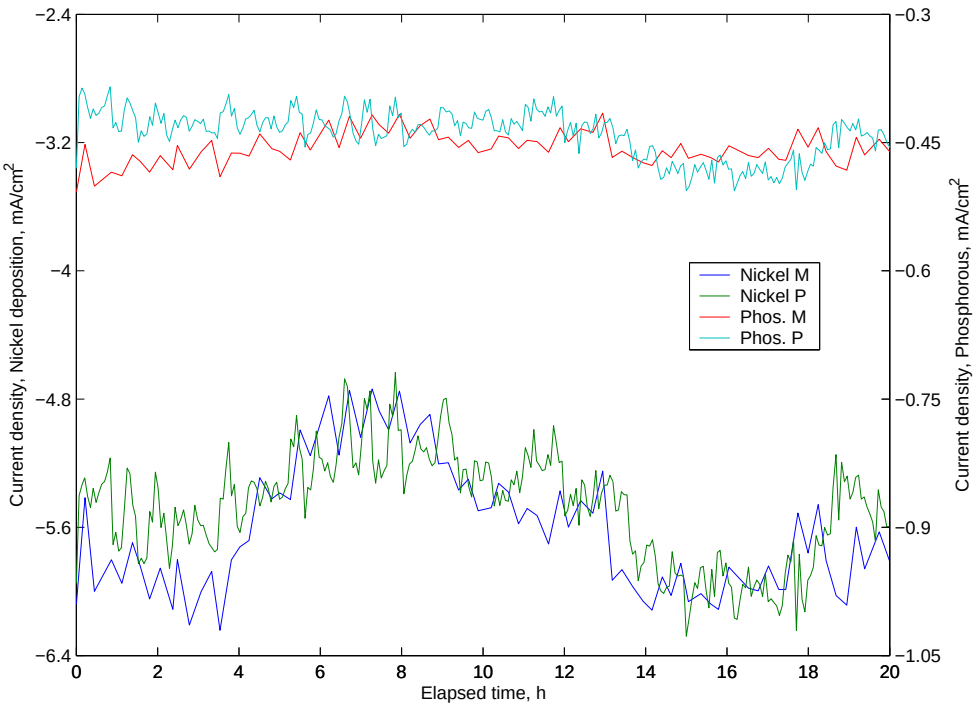

Figure 3.10: Current densities of nickel and phosphorous deposition reactions calculated by measurements (M) and predicted by model (P).

In addition to the electrochemical processes also the unobservable chemical processes, like reaction rates shown in Figure 3.11, can be estimated. The estimates can be used for plating mechanism analysis discussed below.

The alloy thickness and phosphorous content are determined by the deposition rates (Figure 3.11) and plating time (Figure 3.4). The plating time is precise and

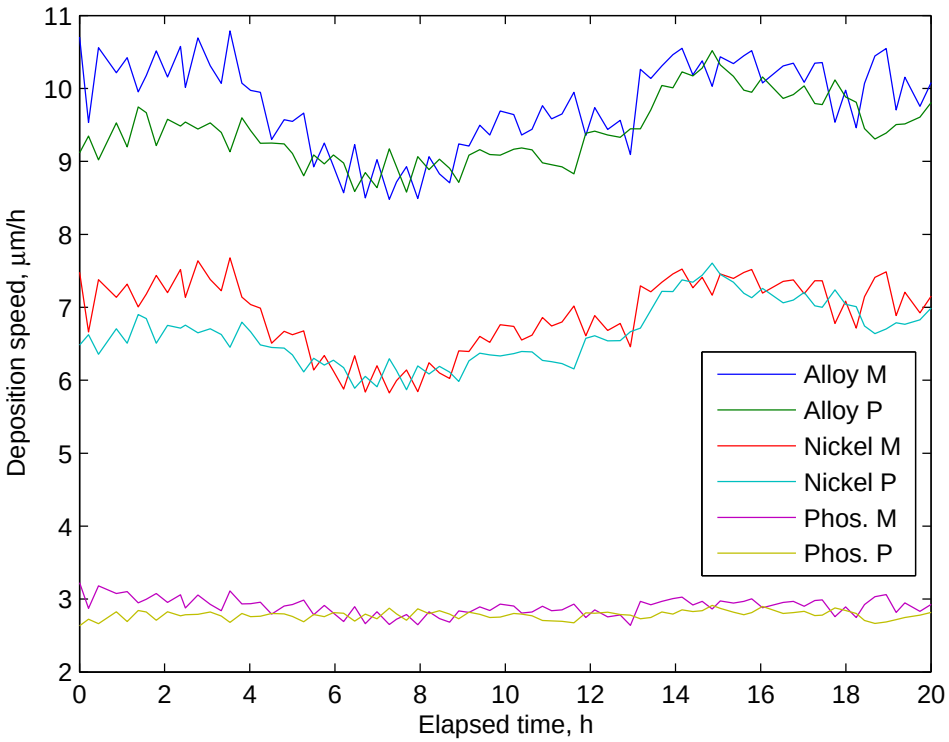

Figure 3.11: Deposition rates.

can be set directly. The plating rates, however, are determined by the current densities which are dependent on the reactant concentrations. The effect of the concentrations is set directly by the empirical constants (2.20)-(2.23) and indirectly by the overpotentials. The effect of overpotentials is more complicated and depends on concentrations, temperature and area through mixed and equilibrium potentials shown in Figure 3.13. The mixed potential is determined by the plating process so that the charge conservation requirement (2.15) is fulfilled. The equilibrium potentials are dependent on the concentrations through Nernst equations (2.16)-(2.19). These complex relations between the nickel and phosphorous deposition reactions and the concentrations are discussed below.

Effect of nickel ion

The nickel deposition rate increases with nickel ion concentration as can be seen by comparing Figures 3.10 and 3.11. This is because the nickel concentration decreases the value of the limitation coefficient (2.23) and decreases the absolute value of the nickel deposition reaction's (2.4) equilibrium potential (2.19) shown in Figure 3.13. Because the mixed potential is not directly influenced by nickel ion

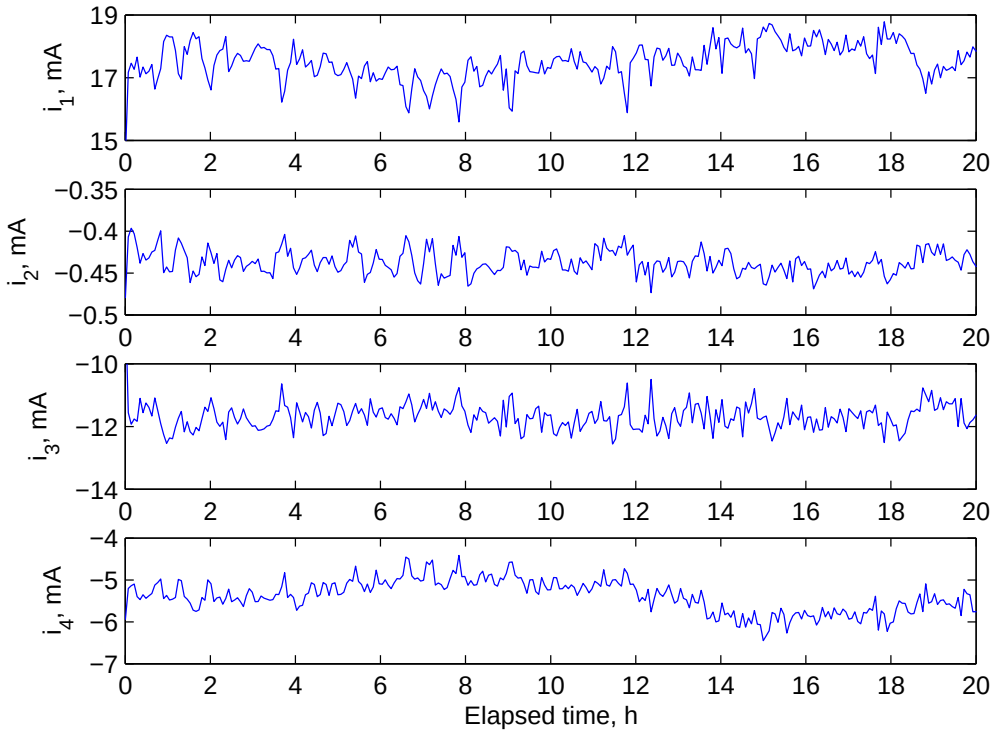

Figure 3.12: Current densities of partial reactions.

concentration, it changes only slightly as can be seen from the Figure 3.1. Therefore, the change in equilibrium potential u_4 increases the respective overpotential, which increases the current density i_4 as shown in Figure 3.12.

The nickel ion concentration has only a minor effect on the phosphorous deposition reaction through a mixed potential change.

The same kind of influences of the nickel ion concentration on the electroless nickel plating reaction dynamics are also observed in [33, 65, 66]

Effect of pH

In previous studies [9, 33, 47, 66, 67] it has been shown that the nickel deposition rate increases if the hydrogen ion concentration decreases (pH increases). The same effect can be seen by comparing Figures 3.9 and 3.11. The reason is the increased activity (2.23) and, in a wider scale, the increased overpotential of the nickel reactions created by the change in mixed potential. The mixed potential change is caused by the more negative equilibrium potentials (2.16)-(2.18), which disturbs the equilibrium of the current densities and, as a consequence of this,

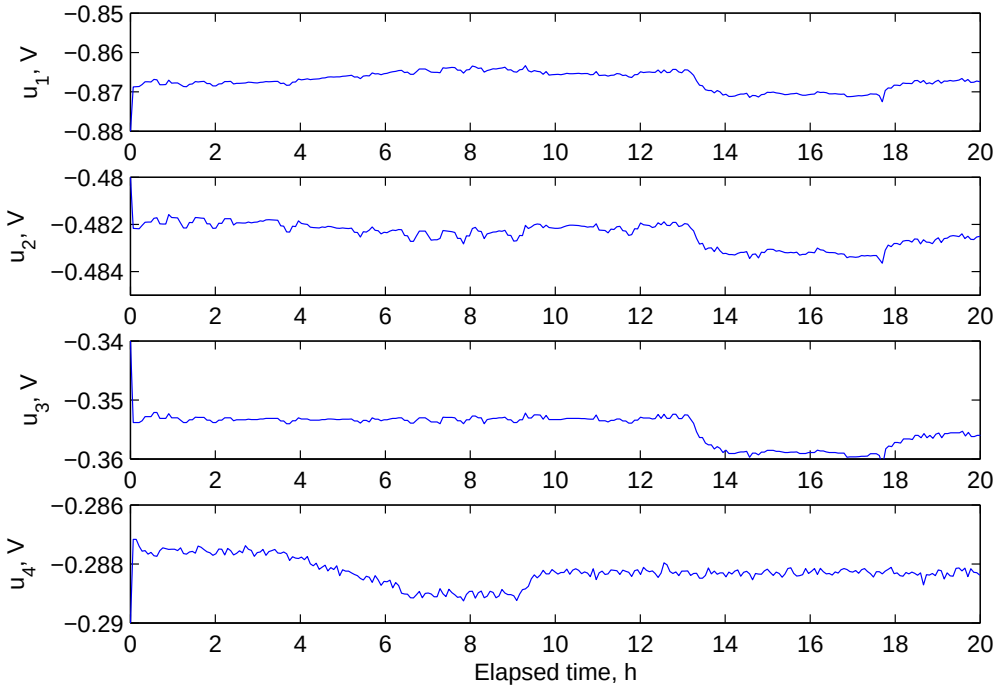

Figure 3.13: Equilibrium potentials of partial reactions.

mixed potential changes so that the electrical neutrality (2.15) is again reached. The effect of the mixed potential change is partly compensated by the raised MTO and therefore this effect is hard to see from Figure 3.1. The increase in the current density of the nickel reaction can, however, be clearly observed from Figure 3.12.

Also phosphorous deposition rate increases along with pH increase as can be seen from Figures 3.9 and 3.11. This is because of the increased activity (2.21) of the phosphorous deposition reaction. The effect is not, however, as radical as on the activity of the nickel deposition reaction (2.23) and therefore the alloy's phosphorous content decreases as shown in Figure 3.6. The increase of the phosphorous deposition rate is limited also by the decreased overpotential of the reaction as can be seen by comparing Figures 3.1 and 3.13. Therefore the phosphorous reaction's current density is increased only slightly if compared to nickel reaction's current density.

In general, higher pH corresponds to higher reaction rates (Figure 3.3 and 3.11) which is exploited in process control to speed up the aged bath [5, 9]. A high reaction rate may cause bath contamination [9, 65, 68] or undesirable film blackening [69] observed frequently in the process.

Effect of orthophosphite

Orthophosphite is only produced, not consumed, by the reaction, as can be seen from equation (2.30) and from Figure 3.7. Therefore, its concentration is related to MTO, which makes it hard to analyze the independent influence of orthophoshite concentration on the reaction kinetic. Maybe because of this, its influence has not been completely analyzed in former studies. The influence can, in some extend, be analyzed by the reaction model as follows. The nickel deposition rate decreases if the orthophosphite concentration increases as can be seen by comparing the Figures 3.7 and 3.11. The effect is seen more clearly if the whole bath lifetime is observed. The reason for this phenomenon is the decreased absolute values of the mixed potential created by the decreased equilibrium potential (2.16) of the oxidation reaction shown in Figure 3.13. The resulting reduction in the overpotential of the nickel reaction diminishes its current density as can be seen from the Figure 3.12.

Also the phosphorous deposition rate reduces along with the orthophosphite concentration increase as can be slightly observed from Figure 3.11. This effect is not, however, so radical if compared to nickel deposition reaction and therefore the phosphorous content of the alloy increases along with orthophosphite concentration as can be seen in Figure 3.6 and observed also in [18]. The reason for the decreased deposition rate and the respective current density is the changed mixed potential, discussed above, which decreases the phosphorous reaction's overpotential.

Effect of hypophosphite

The effect of hypophosphite is hard to see from the Figures, because for productional reasons the dominating nickel ion concentration was changed along with hypophosphite as seen by comparing Figures 3.7 and 3.8. However, the effect of hypophosphite can be explained with the help of the model as follows. The increase of hypophosphite concentration increases the absolute values of the equilibrium potential of oxidation reaction (2.16) and decreases the absolute value of the equilibrium potential of phosphorous reaction (2.17), as can see from the respective equations (the term $\lg c_1$ is oppositely signed in the equations). As a result the mixed potential stays nearly constant. Therefore, hypophosphite has no effect on the nickel deposition rate but increases the overpotential and the reaction rate of phosphorous reaction. Therefore the hypophosphite increases slightly the alloy's phosphorous content. The same kind of behavior is also observed in [9, 33, 67].

3.6 Conclusions

In this Chapter, the developed process model has been tested against independent data gathered from three active and several passive experiments conducted in an industrial PCB manufacturing line. It is shown, that in all the experiments, the model is a relatively good agreement with the measured data and responds correctly to the changes in plating conditions. With the aid of the model, also the complicated reaction mechanism was discussed and explained mathematically. The resulting new perspective is in a good agreement with the literature and former research results.

In addition to these experiments shown in the Chapter, the model has been former validated with two different industrial plating chemistries from different manufacturers. These chemistries produce electroless nickel alloys with a remarkable higher phosphorous contents (10-12 $wt.\%$) than the chemistry shown here (7-10 $wt.\%$). Also in these experiments, the model showed similar accuracy and performance as in the test showed. However, because the additives of the plating chemistries differ greatly from each others, the model had to be re-calibrated separately for each of the chemistries.

Based on these results, it can be stated that the proposed model is capable of estimating the unobservable product and bath parameters of electroless nickel plating process, online from the standard measurements used in circuit board industry. The accuracy, performance and adaptability of the model make it usable for industrial PCB process monitoring and control applications.

Chapter 4

Process Monitoring

4.1 Introduction

A new monitoring system of electroless nickel plating process, used in printed circuit board manufacturing, is presented in this Chapter. The monitoring system is based on the developed electroless nickel model of Chapter 2. It is shown that critical board parameters can be estimated online from standard process measurements of an industrial electroless nickel plating line. Besides product parameters, the model provides online information on the electroless plating bath in terms of the electrical and chemical characteristics, useful for failure source detection and process control.

The proposed model-based monitoring system provides the current process and product parameter states faster and more completely than traditional laboratory analysis based systems. In the case of a failure, it allows fast detection of the failure source, which is essential for failure correction.

4.2 Motivation

The conventional control method in electroless nickel plating is to keep the bath parameters (concentrations, temperature) constant and assume constant reaction rates [5]. However, this is a poor policy in practice, because the process becomes slower during bath aging which can be compensated by a higher pH-level [4, 9]. Also the by-product development and loading changes disturb the reaction rates and the reaction balance [9].

In more sophisticated methods the bath parameters are changed during plating to compensate for the changes. Because the board parameters cannot be measured online, the changes are rough and based on the operator's experience [5].

Problems arise especially when the process is changed and new control rules have to be learned [4].

Nowadays, modern plating lines are computer controlled [70] but despite the intense automation in process industry, the automation level is still low here [3]. Although computer drives the line according to a preprogrammed plating program, the control decisions are still made by the operator and are based on his experience. This is because of complex manufacturing processes and lack of direct product parameter measurements. Especially, in cutting edge production the tolerances are tight, and rough, operation-based control is not acceptable anymore. Therefore, if a fully automatic and accurate process control is not possible at the moment, the plating quality can be improved by providing a more detailed process information to the operator. This kind of new monitoring concept is proposed in this Chapter.

4.3 Contribution

The following contributions are covered in this Chapter:

1. A new, model-based monitoring system for electroless nickel plating process is presented.
2. It is shown that the monitoring system provides an accurate estimate of the process state in terms of alloy thickness, phosphorous content, electrochemical processes and bath concentrations.
3. It is shown that the proposed monitoring model is adequate for state estimation also for multiple baths with different makeup concentrations.
4. It is shown that the solderability measurements are not directly related to phosphorous content but affected by other process parameters also.

4.4 Monitoring system

The monitoring system is based on the developed process model presented in Chapter 2. The data flow chart of the model is shown in Figure 4.1. The model allows online estimation of the product parameters (film thickness, phosphorous weight percentage), along with the electrochemical parameters (deposition speed, mixed and equilibrium potentials, current densities) and the chemical parameters (reaction rates, hypo- and orthophosphite density, hydrogen gas evolution rate) from the online measured pH, nickel concentration, flow rates, bath temperature, plating time and bath loading.

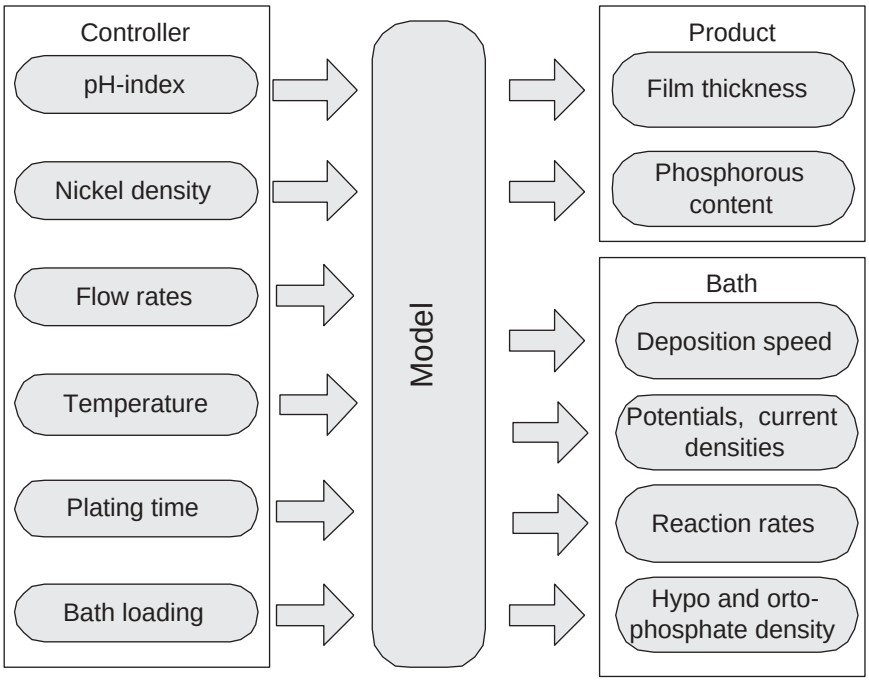

Figure 4.1: Model based process monitoring system.

The process monitor is integrated to an industrial process control system where it is in interaction with the plating bath through the intermediate layer for the bath controller and a flightbar controller as shown in Figure 4.2. For history analysis, it has also access to the laboratory analysis database. Each of the system elements has multiple functionalities, discussed in the following.

Bath controller This controller keeps the plating chemistry in balance by controlling the pH to follow a target profile and keeping the nickel concentration at a constant level.

Flightbar controller This crane controller moves the plates from one bath to another according to a preprogrammed schedule. It manages the logging register and takes care of the bath temperature.

Laboratory database The laboratory analysis carries out the final quality checking and supervises operators if corrections are required. The quality checking is based on the product parameter analysis from the plated products where the film thickness is measured with a XRF analyzer, wetting time and force with wetting balance analyzer. If unsuitable quality is observed the lot is discarded.

The laboratory analysis include also the bath parameter supervision: the pH and nickel concentration analysis every 4 hours and the hypophosphite concentration every 6 hours. If some systematic deviation between the online measurements and the laboratory analysis is discovered, the controllers are re-calibrated.

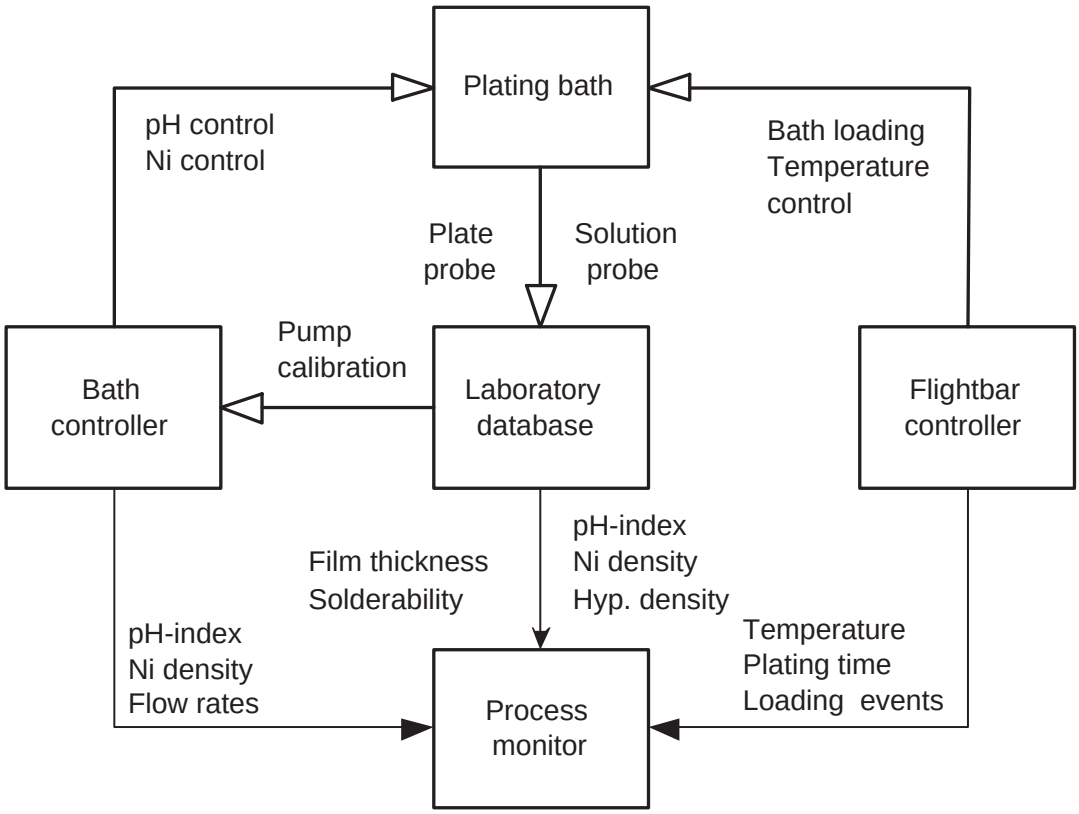

Figure 4.2: The monitoring system where the monitoring engine is integrated with the plating bath through the intermediate layer.

Process monitor This computer characterizes the process state in terms of electrical, chemical and board parameters as shown in Figure 4.1. The system can also represent the plating history of the previous batches up to the current moment to be compared with the results measured later in the laboratory analysis.

4.5 Monitoring results

The proposed monitoring system was tested retrospectively on a large sample of industrial data shown below. The data represent the bath behavior during six baths.

Deposition precesses

In Figure 4.3, the estimated and measured film thicknesses are shown. The film thicknesses were measured by using two different methods. The XRF measure-

ments (also known as coating thickness measurements, CMI), give a high resolution measurement of the thickness while the validity of these values and the calibration of the XRF analyzer were secured by low resolution (0.5 μm) thickness measurements from the cross section of a sample (marked in the figure as HIE) by using an optical microscope. The estimated and the XRF measured film thicknesses are relatively close each other. There are still periods where the values differ from each other. The reason might be inaccurate measurements or exceptional changes in process conditions, like manual additive additions. Unfortunately, the sparse set of measurements prevents a more accurate analysis. The most accurate measurement would be gathered by cross section analysis using SEM, but it would be too time consuming and expensive for production purposes.

Figures 4.3 and 4.8 reveal the relation between the estimated film thickness and the MTO, which is natural; the higher the by-product or the orthophosphite concentration the lower the deposition rate. This phenomenon can be compensated by raising the pH respectively as shown in Figure 4.7. As can be observed, the target profile depends stepwise on the MTO currently. However, more stable deposition rates can be reached by a better choice of the pH target profile [61].

The peak values of thickness can be explained with the start-up pH of the bath and the corresponding peaks of the measured nickel concentration which can be observed in the Figures 4.7 and 4.9, respectively. The rapid oscillation is because of the changes in bath loading and plating time.

In Figure 4.4, the estimated phosphorous weight percentage is shown. The phosphorous weight percentage measurement is not included in the standard process measurements and therefore, no reference values are presented. However, by comparing Figures 4.4, 4.7 and 4.8, the known relation between phosphorous content and the pH and MTO can be confirmed implying the system's validity. The peak values of phosphorous may be explained with the corresponding peaks of the measured nickel density and the start-up concentrations of a new bath, as was the case also in film thickness.

A wetting balance measurement is included in the standard measurements and the results are shown in Figure 4.4. Time T is the time in seconds in which the solder reaches 2/3 of its maximum force. Forces F1 and F2 are the solder's maximum forces in mN at 2 and 4 seconds after soldering. The wetting parameters are shown in same scale, which is seconds for the wetting time T and mN for the wetting forces F1 and F2. According to literature [9, 18, 29, 30, 71], the phosphorous content characterizes the inner stress and corrosion resistance of the film and is closely related to PCB solderability. Besides phosphorous, solderability is affected also by many other factors like the cleanliness of the surface, board aging at high temperature, nickel concentration in gold bath and gold thickness after final plating. Because of these, the phosphorous content shows only some weak correlation with the wetting time (correlation coefficient = 0.14) and almost

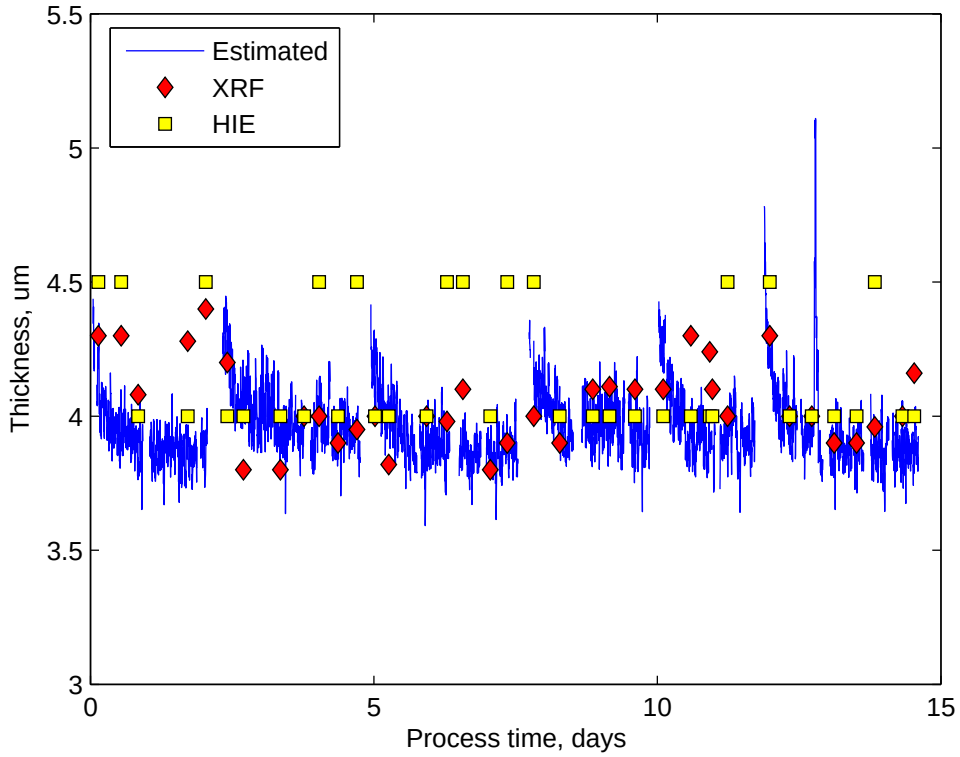

Figure 4.3: The online estimated, XRF measured and optical cross section (HIE) measured alloy thicknesses. The reference value for the thickness was 4 μm

.

no correlation (-0.028, -0.023) with the wetting forces. Therefore, it seems that against the common notion, the phosphorus content of the film is a poor indicator for these characteristics.

Electrochemical processes

Electrochemical processes form the basis of the plating reaction and therefore some critical reaction parameters, like partial processes state and balance, can be observed by monitoring the electrochemical processes. The current densities and equilibrium potential along with the mixed potential are presented in Figures 4.5 and 4.6. The unbalance of these partial processes indicate bath contamination the reason of which can be derived from the states of the partial reactions. If this information is provided to the operator, possible problems can be reacted properly and more quickly than is the case with the traditional monitoring system.

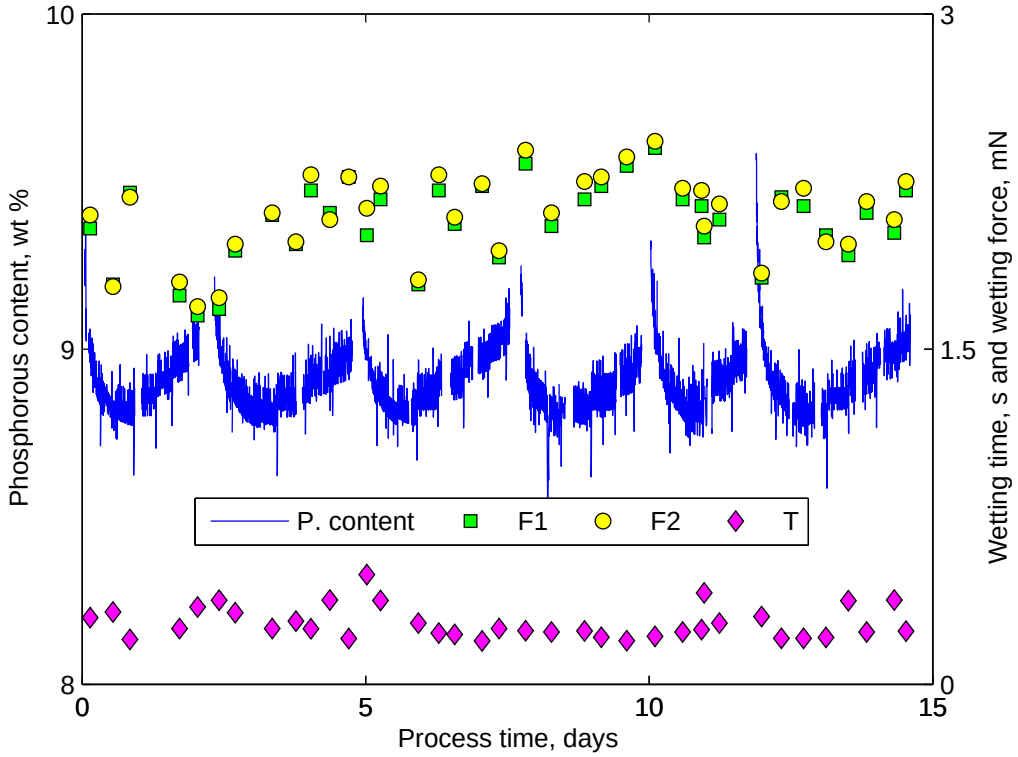

Figure 4.4: The online estimated phosphorous content in wights percentages along with the measured wetting time (T) in seconds and wetting forces (F1, F2) in mN. The reference value for the phosphorous content was 9 $wt.\%$

.

The overpotential, i.e., the voltage between the mixed potential and equilibrium potentials shown in Figure 4.6, controls the current densities of the partial reactions shown in Figure 4.5. The current densities are related to the deposition speeds of nickel and phosphorous and eventually to the film thickness and phosphorous content shown in Figures 4.3 and 4.4, respectively. Therefore, problems in these product parameters can be observed early by monitoring the electrochemical reactions. The curves shown in the figures are typical for well-balanced processes indicating that the phosphorous is evenly distributed over the nickel layers. The higher reaction rates in the beginning of the baths are due to the initial concentrations and process start up.

It can also be seen that the peak values of the current densities in the middle of the last bath are mainly caused by the high pH, shown in Figure 4.7, and the peak in the nickel concentration, shown in Figure 4.9. These parameters are over their references in that point, which increases the activation coefficients (2.20)-(2.23) and further the respective current densities. Especially, the nickel

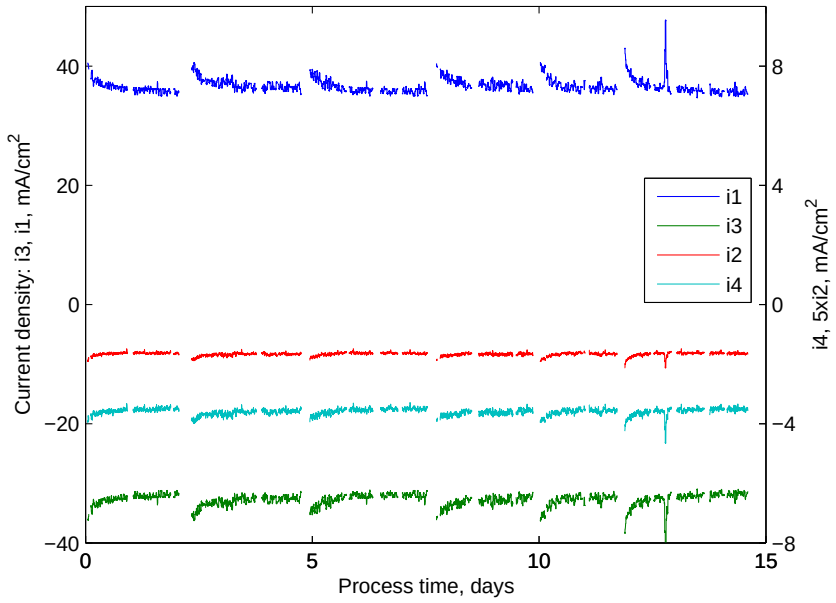

Figure 4.5: The online-estimated current densities of the reactions.

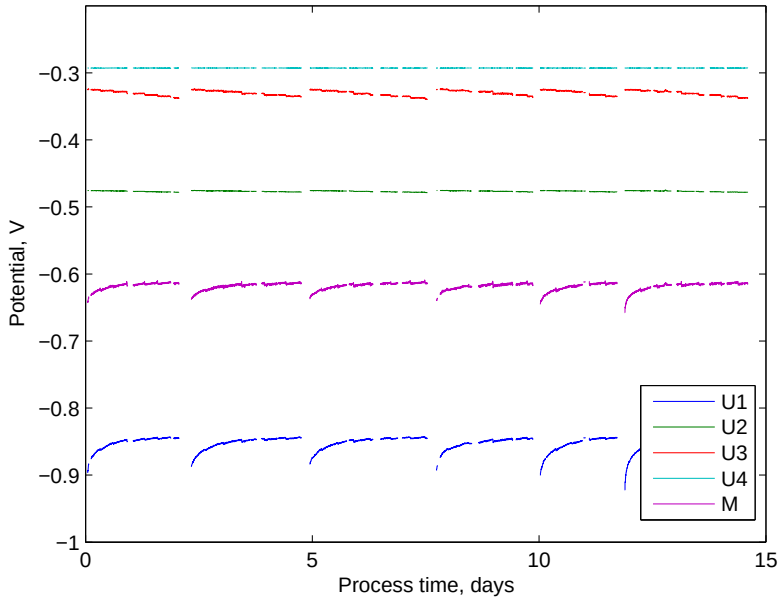

Figure 4.6: The online estimated mixed potential (M) and the equilibrium potentials u_1, u_2, u_3 and u_4 of the reactions.

deposition rate is high in that point because both of these parameters have an effect on the activation coefficient of the nickel reaction (2.23).

The radical raise in the nickel current density has also an effect on the other current densities because of the electrical neutrality requirement (2.15). The electrical neutrality is reached through the changes in mixed and equilibrium potentials, as discussed earlier. However, the effect of the this is relatively small as can be seen from Figure 4.6, where the potentials are almost unchanged and no significant change in the polarizations of the reactions is observed in that point.

Because the plating time was not changed in that point, the effect of the current density peak can be seen also from the film thickness, shown in Figure 4.3. No respective peak can be found from the phosphorous content, shown in Figure 4.4, which confirms that this unbalance of concentrations affects especially the nickel reaction.

The bath unbalance, which change the reaction polarization and is involved in the bath contamination, could be observed through a radical change in the level of the mixed potential shown in Figure 4.6.

Concentrations

In Figures 4.7, 4.9 and 4.10 the model estimated pH, nickel and hypophosphite concentrations are presented along with the respective online and/or laboratory analysis. The concentrations of the species control the partial reaction rates, which is exploited in process control. Especially the pH is crucial. It is used to compensate the reaction deceleration, caused by the by-product formation and bath aging, in the manufacturing line. Therefore, it is adjusted according to the MTO as can be seen from Figures 4.7 and 4.8. The model predicted and measured pH-indexes are in relatively good agreement with each other and in moderate agreement with the results measured later in the laboratory.

The nickel concentration can also be used for process control, but in normal conditions it is kept constant by the bath controller. Because of the importance of nickel concentration, its value is measured also in the laboratory and the bath controller is calibrated according to these results. The disagreement of the measurements can be seen from Figure 4.9 where also the model estimated value is presented. The estimated value shows good agreement with the bath controller but not with the laboratory analysis. The reason for that might be an error in the volume flux measurement of the nickel sulphate addition. However, if the laboratory measurements are kept as the most precise ones, it is noteworthy that the estimate seems to be more accurate than the bath controller.

The hypophosphite concentration, shown in Figure 4.10, has also an effect on plating reaction, but it is not as critical as pH or nickel concentration and therefore

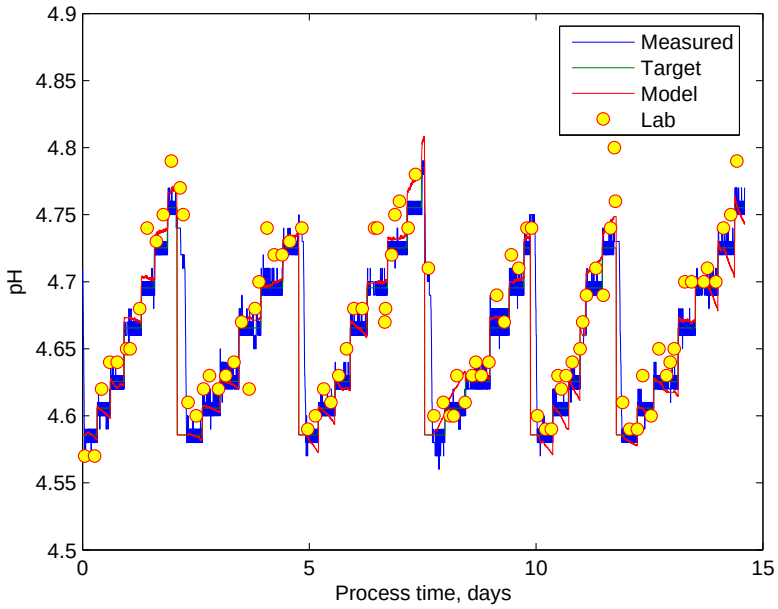

Figure 4.7: The measured, model-predicted and laboratory-analyzed pH.

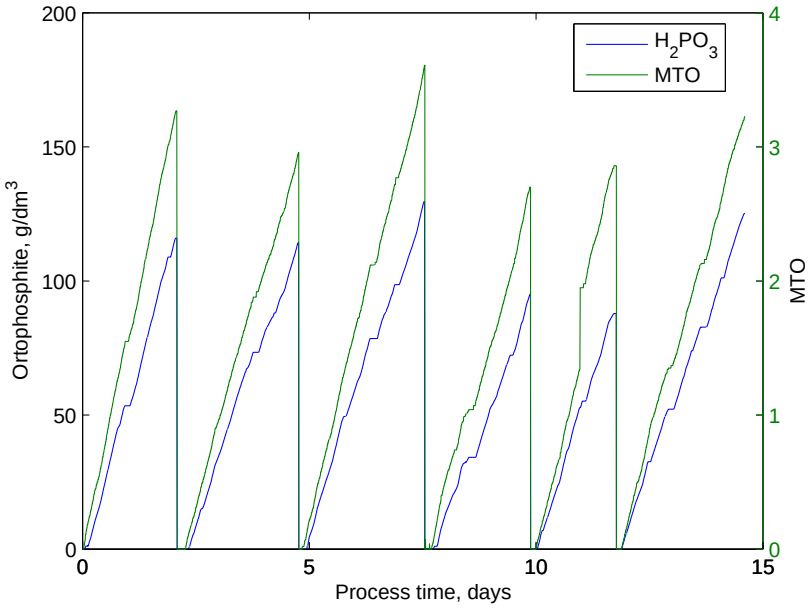

Figure 4.8: The measured metal turn over (MTO) and online estimated orthophosphite concentration.

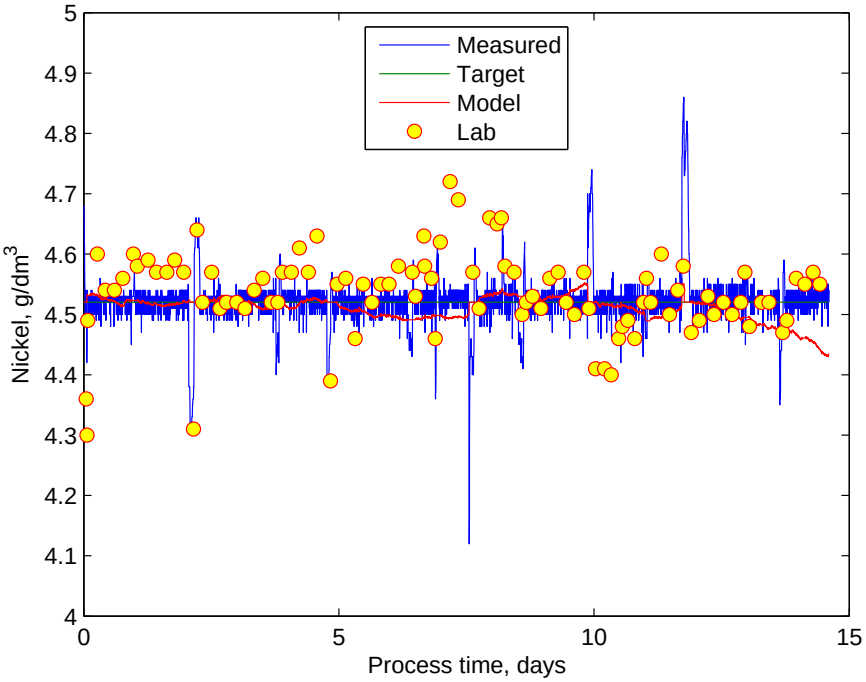

Figure 4.9: The measured, model-predicted and laboratory-analyzed nickel concentration.

it is analyzed in the laboratory less frequently. In general, the model predicted hypophosphite concentration seems to be close to the laboratory analysis and the estimate error stays below 5 % of the target value (35 g/dm^3). However, between the days 5 and 7 the estimate error raises up to 14 % of the target value, which cannot be explained based on the used measurements. One error source might be the volume flux measurement of the hypophosphite addition. In the studied process the hypophosphite is assumed to be consumed at the same rate as nickel, while the aim is to keep these concentrations constant. Therefore the bath controller does not control hypophosphite concentration itself but hypophosphite is added along with and related to nickel additions. This strategy is not very successful as can be seen from the figure, where the measured values change vigorously. Also, if the Figures 4.9 and 4.10 are compared, almost no correlation can be seen between the laboratory analysis of nickel and hypophosphite concentrations, which implies that the nickel and hypophosphite consumptions are not related. This is evident, if the reaction mechanism (2.1)-(2.4) is observed. There the nickel takes a part only in one reaction (2.4) while hypophosphite is involved in two reactions (2.1) and (2.2). This contradiction implies the need for the more sophisticated process control, in which also the hypophosphite concentration is taken into account independently.

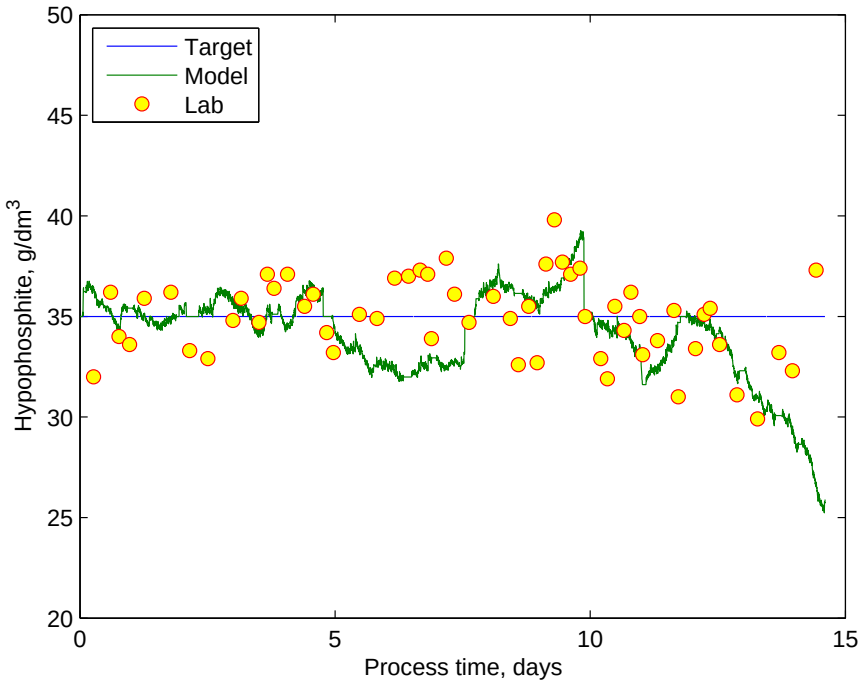

Figure 4.10: The online-estimated hypophosphite concentration, compared to the results measured later in a laboratory.

4.6 Conclusions

A novel monitoring system for electroless plating process was presented in this Chapter. The monitoring system characterizes online the complex process of electroless nickel plating in terms of the electrical, chemical and product parameters from standard PCB industry measurements, using the process model discussed earlier in Chapter 2. The monitoring system provides online the same data that is normally measured afterwards in the laboratory analysis. In addition, it provides estimates of alloy's phosphorous content and electrochemical parameters, which are critical for the effective process control, but unfortunately unobservable in normal process control.

The monitoring system provides all the critical information of the plating process in a clear and compact form, offering fast preprocessing. Therefore, it enables a fast failure detection and correction, which is essential in PCB manufacturing.

The monitoring results may also be used for the process model validation if respective measured values are available. In these cases, the process model showed good agreement with the measured values with multiple baths having different initial concentrations and loading profiles.

Therefore, it can be stated, that the proposed monitoring system is capable of state estimation of an industrial electroless nickel plating process. Also the accuracy of the proposed process model is shown to be adequate to be used in applications on an industrial plating process.

Chapter 5

Process Control

5.1 Introduction

Electroless nickel is commonly used coating in many industries like oil and gas industry, machinery, etc. [9]. In these traditional applications the alloy properties are not critical and no accurate process control is needed. Maybe, this is why there is no effective automatic control available for the electroless nickel plating. However, in new electroless nickel applications, like in printed circuit board or semiconductor manufacturing, the requirements for the alloy are strict and tolerances tight, e.g., in PCB manufacturing, electrically isolated contactors are only a few microns thin and packed close to each other. To plate these the traditional operator based process control is not adequate but a more precise control is required [30].

In this Chapter a control algorithm of electroless nickel plating process is proposed. The control algorithm is designed especially for PCB manufacturing where it is capable of stabilizing the critical board parameters i.e. the thickness of the plating film and its phosphorous content, at desired levels by controlling the pH and the nickel ion concentration of the plating bath. The algorithm can, however, be applied also for other applications of electroless nickel plating. The algorithm consists of optimal trajectory calculation for pH and nickel ion concentration and a feedforward PI-control by which the trajectories are reached. The trajectory calculation is based on the process model described in Chapter 2. Besides an effective process parameter control, the control algorithm keeps the process in balance avoiding a spontaneous bath decomposition caused by the unbalance of pH, nickel source or reducing agent concentrations [65, 68, 72].

Electroless nickel plating is a highly disturbed process by the bath loading [46, 73, 74]. In addition to the fact, that the existence of loading, i.e. the substrate, is essential for the progress of the plating reaction, it determinates the total reaction

and reagent consumption rates affecting, therefore, radically to the plating parameter and disturbing the bath's balance. In this Chapter a new control scheme is developed. The scheme is capable of eliminating the disturbances affected by the loading process.

5.2 Controlling history of electroless nickel plating process

The traditional way to control the electroless nickel plating process is manual. This kind of process control is found to be adequate in traditional applications like in oil and gas industry or machinery were the alloy is used only for corrosion protection. While the applications have become more challenging, the interest in automated process control has increased [5]. Because of the complexity of the process and the ignorance of its precise mechanism, the automation level is still low and control is more or less operation based.

The most usual way to control the process is to keep the bath parameters constant and assume constant reaction rates [5]. However, this is not the case in practice because, although the concentrations and temperature could be kept constant, the bath loading would change disturbing the reaction [46, 73, 74]. Even if the loading would be constant, the by-product deposition and bath aging disturb reaction reducing reaction rates [9].

In more sophisticated control strategies the bath aging is compensated by increasing the pH stepwise according to MTO as shown in Chapter 4. This strategy is still inaccurate and does not control the phosphorous content of the alloy. It actually inflicts a pareto optimization problem between the alloy thickness and phosphorous content. This is because the raise of pH increases the alloy thickness and lowers its phosphorous content and *vice versa*, as discussed earlier in Chapter 3 and discovered also in [9, 33, 47, 66, 67]. Therefore, it is impossible to control accurately both the parameters applying only pH control. This concept does neither take into account the by-product deposition which decrease the plating rates and might result in bath contamination [9, 46, 75].

Although the previous control strategy is used in PCB manufacturing, there is a need for more precise control [6]. The controller should be capable of controlling both the alloy thickness and its phosphorous content separately. It should also be capable of preventing bath contamination and by-product effects. That kind of new control algorithm is proposed in this Chapter.

5.3 Contribution

The following contributions are covered in this Chapter:

1. An effective new control algorithm for the electroless nickel plating process is developed.
2. The applied tracking trajectory is electrochemically balanced, relevant to the global target and to the current state of process. Therefore, the proposed tracking control keeps the process in balance and avoids the spontaneous bath decomposition caused by the unbalance of pH, nickel source or reducing agent.
3. It is shown that the alloy thickness and phosphorous content can be controlled by controlling the pH and nickel ion concentration of the bath.
4. Tracking of the nickel concentration and pH allows separate control of the film thickness and phosphorous content. Their control is not in disagreement anymore as it was when a single control (pH) is applied.
5. The algorithm compensates the disturbances due to the bath loading. The known state of loading switches controls faster than its aftereffect in pH or nickel concentration.

5.4 Control strategy

In printed circuit boards, the thickness and phosphorous content are the prime parameters of electroless nickel alloy [3, 9, 22]. Unfortunately, these are unobservable and analyzed afterwards in the laboratory with a delay not suitable for effective control [73, 76]. A better control method is to evaluate these parameters from online measurements according to the process model presented in Chapter 2. The estimates are then applied for calculation of the electrochemically balanced tracking trajectories of the pH and nickel ion concentration which are observed to have an effect on the parameters [9, 33, 47, 65, 66, 67]. The trajectories can be reached by controlling ammonia and nickel sulfate pumping accordingly. A schematic diagram of the proposed control concept is described in Figure 5.1.

This stabilization control is completely automatic and its reference values are obtained from current process state. This control strategy is contradictory to the traditional method in which the references are set heuristically based on the delayed laboratory analysis. It also enables separate control of the alloy thickness and phosphorous content abrogating the disagreement between the control of these two parameters, which exists if the traditional single pH control is applied.

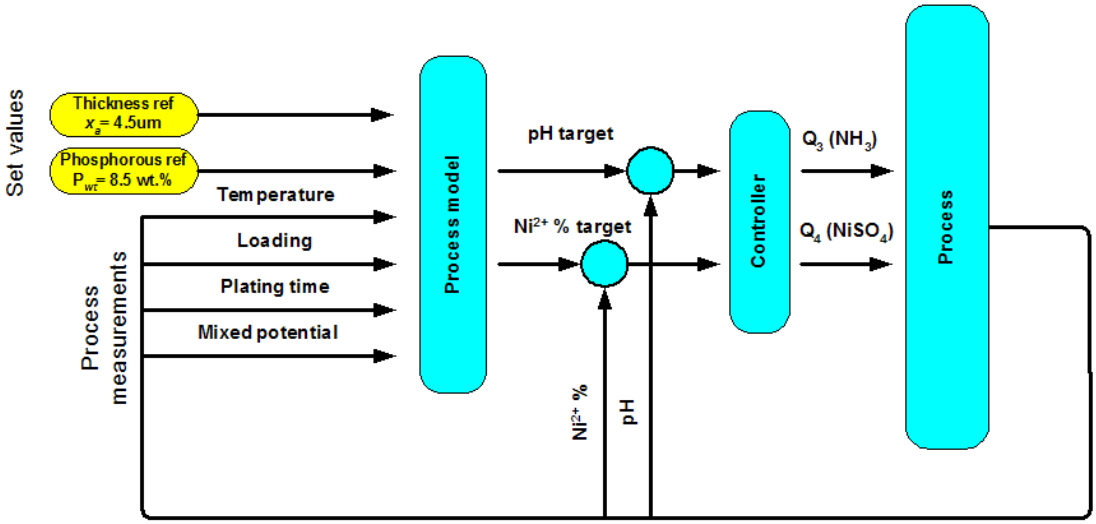

Figure 5.1: The schematic diagram of control system [4].

5.5 Optimal trajectory

The desired thickness of the plated Ni-P-alloy film is a constant equal to the central point of the admissible range, $x_a = 4\ \mu m$, while the desired phosphorous content is $P_{wt} = 8.5$ wt.% [3, 9, 22]. The partial thicknesses of nickel and phosphorous can be calculated as target values for the control from the desired alloy thickness and its phosphorous content:

$$x^*_{Ni} = x_a - x^*_P \qquad x^*_P = x_a P_{vol}/100, \tag{5.1}$$

where
x^*_{Ni} - target thickness of nickel, cm,
x^*_P - target thickness of phosphorous, cm.

These targets can be achieved and the bath contamination is avoided if an electrochemically balanced tracking trajectory is used for adjustment of the pH and nickel percentage. The balanced trajectory is calculated through the electrochemical system including the charge conservation requirement (2.15), the electrode reactions (2.10-2.13) and the thermodynamic equilibrium potentials (2.16)-(2.19). It includes also the deposition rate (2.26) and target (5.1) requirements, coupled with the relationship

$$-\frac{i_4}{C_{Ni}} = \frac{x^*_{Ni}}{t}, \qquad -\frac{i_2}{C_P} = \frac{x^*_P}{t}, \tag{5.2}$$

where

C_{Ni}, C_P - volumetric charge densities of nickel and phosphorous, C/cm^3,

$$C_{Ni} = \frac{2F\rho_{Ni}}{M_{Ni}}, \qquad C_P = \frac{F\rho_P}{M_P}. \tag{5.3}$$

A target value for the current densities i_2 and i_4 can be solved from equation (5.2). These target values can further be compared to the model estimated current densities dependent on pH and nickel ion concentration. To keep the reaction balanced, the charge conservation requirement (2.15) has to be fulfilled throughout the process. This prevents that no reaction is over-accelerated by excess nickel source or ammonia pumping, which would result in bath decomposition [65, 68, 72].

The simplest way to calculate the electrochemically balanced trajectory is to minimize numerically the function

$$f(i_{1,\dots,4}(c_3, c_4, \phi)) = (i_1 + i_2 + i_3 + i_4)^2 + (i_2 - C_P\frac{x_P^*}{\tau})^2 + (i_4 - C_{Ni}\frac{x_{Ni}^*}{\tau})^2 \tag{5.4}$$

with respect to hydrogen and nickel ions concentrations, c_3 and c_4, respectively, and mixed potential ϕ. Therefore, the balanced trajectory is a triple of the hydrogen and nickel ions concentrations and mixed potential as presented in the following. Here the hydrogen ion concentration is presented as pH ζ_3 and nickel ion concentration is presented as nickel percentage ζ_4, meaning that 100 % is equal to 0.1 mol/dm^3 Ni^{2+}.

$$\zeta_3 = -\lg c_3(c_1, c_8), \qquad \zeta_4 = 10^3 c_4(c_1, c_8), \qquad \phi = \phi(c_1, c_8). \tag{5.5}$$

where
ζ_3 - optimal trajectory of pH,
ζ_4 - optimal trajectory of nickel percentage.

The mixed potential cannot be directly controlled but it is set by the deposition process itself or more specifically by the reactant concentrations [73]. Therefore the only possible control parameters are the pH and nickel percentage which are also dependent on hypo and orthophosphite and implicitly on mixed potential via complex electrochemical dependencies.

The plating process is well controlled and in balance as long as the target concentrations ζ_3 and ζ_4 fulfill the requirement (5.4) with real mixed potential. Otherwise a change of the mixed potential takes place in bath effecting all the reactions. Unfortunately, this change takes place even if the pH and nickel percentage are kept constant because the hypo and orthophosphite concentrations are never constant. Besides feeding rates they depend on the utilization and consumption rates.

Therefore, to control the alloy thickness and phosphorous content, the pH and nickel percentage cannot be kept constant but forced to follow the time-varying optimal trajectory. This tracking control problem is solved next.

5.6 Tracking control

The thickness and phosphorous content of the plated film can be kept at the desired levels by tracking the optimal trajectory of the pH and nickel percentage discussed above. The simplest way to solve this tracking problem is to use the following feedforward PI-control u_t:

$$u_t = A_p z_t \upsilon - K_P[\xi_t - \zeta_t + \frac{1}{T_i}\int_0^t (\xi_s - \zeta_s)ds], \tag{5.6}$$

where

ζ	-	optimal tracking trajectory vector, $\zeta = [\zeta_3, \zeta_4]^T$,
ξ	-	vector of measured pH and nickel percentage, $\xi = [\xi_3, \xi_4]^T$
u_t	-	control: vector of ammonia and hypophosphite/nickel feeding rates, $u_t = [Q_{3f}, Q_{4f}]^T$,
A_p	-	maximum loading, dm^2/dm^3,
z_t	-	bath loading level, $z_t = Z/N$,
Z	-	state of loading, Z=(0, ... ,2),
N	-	maximum number of racks in use, N=2,
υ	-	setpoint for control fluxes,
K_P	-	control gain, diagonal matrix of weights,
T_i	-	integration time.

The parameters have to be tuned depending on the bath volume and other process parameters. In tuning, it is noteworthy, that overshoot is not desirable, because the control is based only on chemical additions. Therefore, the excess chemical cannot be pumped out from the bath but the process has to consume it. The overshoot of nickel percentage and pH might also cause bath contamination. Therefore, if the levels have to be changed radically and the capacity of peristaltic pumps is low, the integrating term of the controller might saturate and an integrator antiwindup has to be applied to the controller. To fulfill these requirements, the parameters K_P and T_i of the PI-controller can be tuned by minimizing the following cost function vector J.

$$J = \begin{bmatrix} J_3 \\ J_4 \end{bmatrix} = \int_0^{t_{end}} \begin{bmatrix} (\xi_3 - \zeta_3)^2 + \frac{0.001}{1+\exp(-1000(\xi_3-\zeta_3))} \\ (\xi_4 - \zeta_4)^2 + \frac{0.01}{1+\exp(-1000(\xi_4-\zeta_4))} \end{bmatrix} dt, \tag{5.7}$$

where

J_3 - cost function of pH,
J_4 - cost function of nickel percentage,
t_{end} - end time of the calibration sequence, s.

The cost function is basically the square of the error signals but it contains also the sigmoid of the error signals, which gives more weight for the error in which the actual pH or nickel percentage is over the optimal trajectory. This limits the overshoot of the controls and prevents situations in which the control is ineffective.

The control is related to the process model only through the electrochemically balanced tracking trajectory, relevant to the target values and to the current state of process, which makes the control robust. The known state of loading is fed forward to control. This is a faster and more stable control than if the loading effect is compensated through the pH or nickel measurements. The tracking control of nickel percentage and pH allows a separate control of the film thickness and phosphorous content. Their control is not in disagreement anymore as it is when a single control (pH) is applied. The efficiency of the proposed control scheme is demonstrated through a simulation experiment discussed below.

5.7 Control simulation

The proposed control (5.1)-(5.6) is tested in a series of simulation experiments, of which one is presented. During the simulation the control corrects the initially low thickness $x_a = 3.7\ \mu m$, and phosphorous $P_{wt} = 7.8\ \%$ up to the target values $x_a = 4\ \mu m$, $P_{wt} = 8.5\ \%$. The target value for thickness is then elevated to $x_a = 4.3\ \mu m$ and then returned to the optimal value. Respectively the target value for phosphorous content is later reduced to $P_{wt} = 8.2\ \%$ and returned to the optimal value. The behavior of the reference trajectories can be seen in Figures 5.3 and 5.4.

The real process conditions is simulated by introducing some realistic disturbances. As in the real process, also in the simulator the main disturbance is bath loading. Because the loading can be assumed to be a discrete process where the state of the loading changes between certain levels, it can be reliable simulated by a finite state Markov jump process. The loading, simulated by using Markov process, is shown in Figure 5.2. In addition, every partial process is also exposed to a Wiener process with a 5 % noise-to-signal ratio, to simulate the uncertainty of the measurements.

The reference and controlled values of the alloy thickness and phosphorous content are shown in Figures 5.3 and 5.4. The controls, i.e., pH and nickel concentrations along with the optimal trajectories and respective control addition are shown in Figures 5.5 and 5.6. In Figure 5.6 the nickel concentration is presented as percents with 100 % corresponding to 0.1 $mol\ Ni^{2+}/dm^3$. Despite the perturbations, the

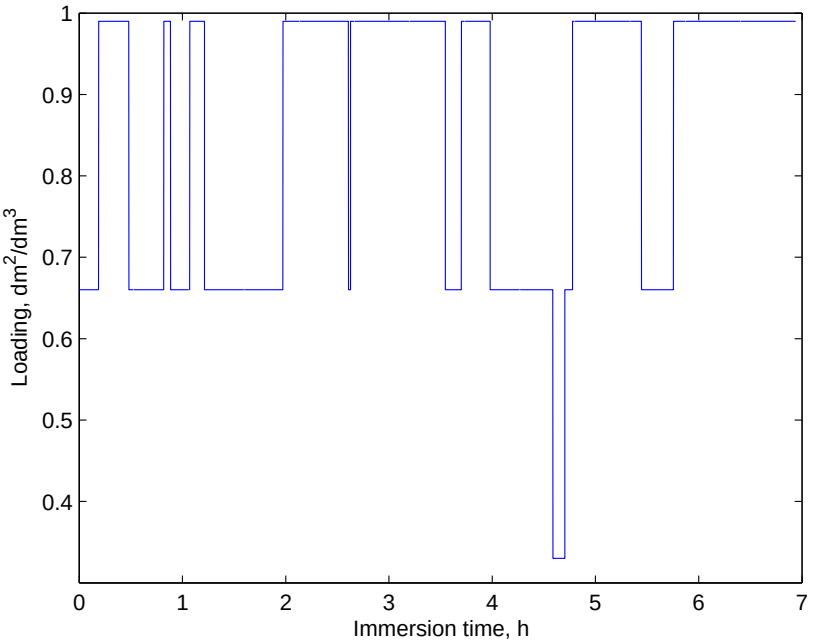

Figure 5.2: Simulated bath-loading process.

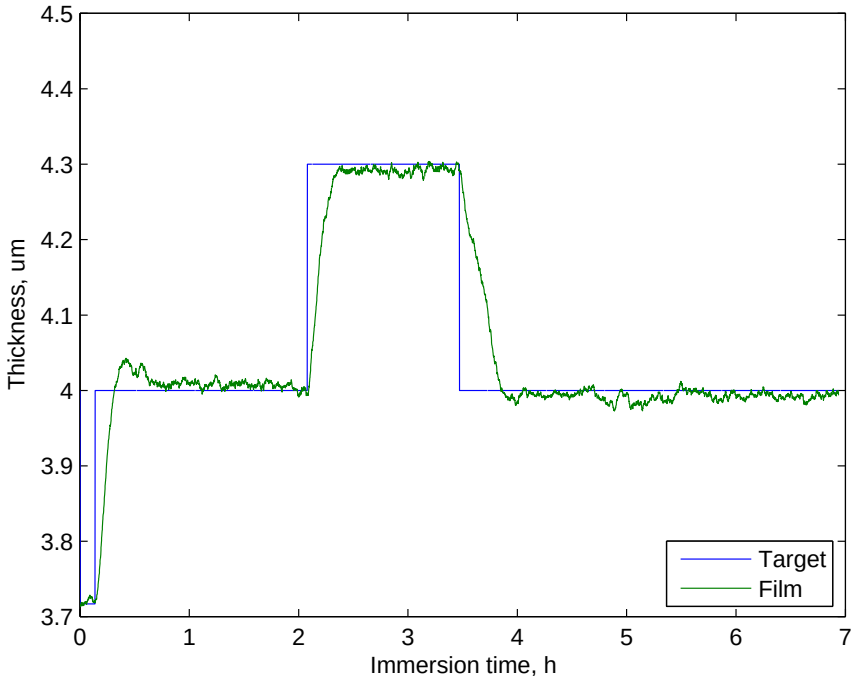

Figure 5.3: Reference and controlled alloy thickness.

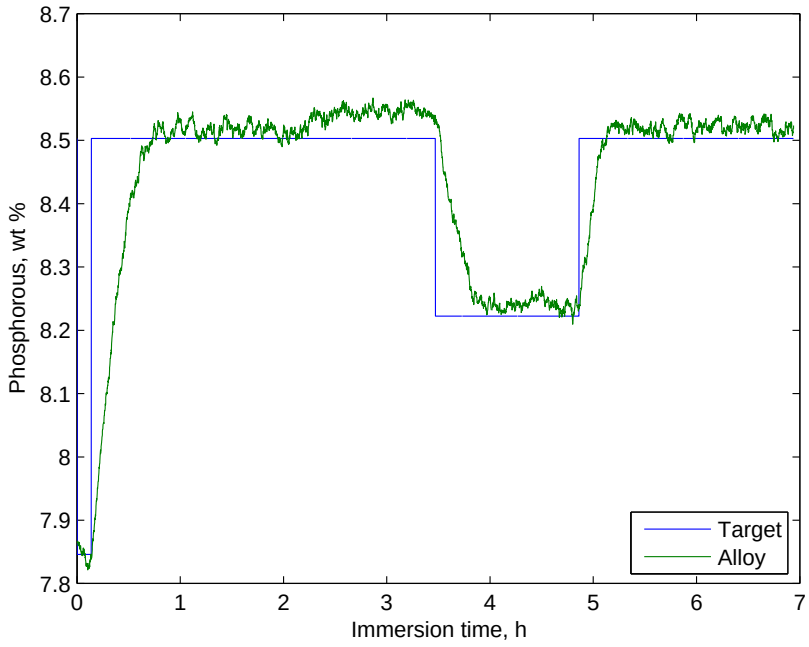

Figure 5.4: Reference and controlled phosphorous content of the alloy.

proposed control is able to stabilize the alloy thickness and phosphorous content at the desired levels regardless of the vigorous reference changes. Only small changes in the feeding rates are required as can be seen from the figures.

Especially alloy thickness control is effective but it also has a slow response in stepwise level changes. This is because of the limited gain of the PI-control preventing the overshoot of the concentrations and because of onesided control of the concentrations. The onesided control means that the nickel concentration and pH can only be increased by the control additions while the decreasing rate is set by the loading which cannot be used for control during production.

In phosphorous content graph (Figure 5.4), the effect of the onesided control can be seen clearly. In the beginning, when phosphorous content is raised to the desired level, the control is delayed. This is because of the slow decreasing rate of nickel concentration shown in Figure 5.6, caused by the low loading as shown in Figure 5.2. The pH, on the other hand, is effectively controlled and the response is rapid even when the level is reduced as can be seen from Figure 5.5. This shows how much the reaction produces excess hydrogen ions, lowering the pH. Also the bath loading level is high at that moment adding the hydrogen ion production.

In practice the control is accurate and reasonable considering that the aim of the control is to keep the alloy thickness and phosphorous content constant without such large level changes. The simulation shows also that the main error source

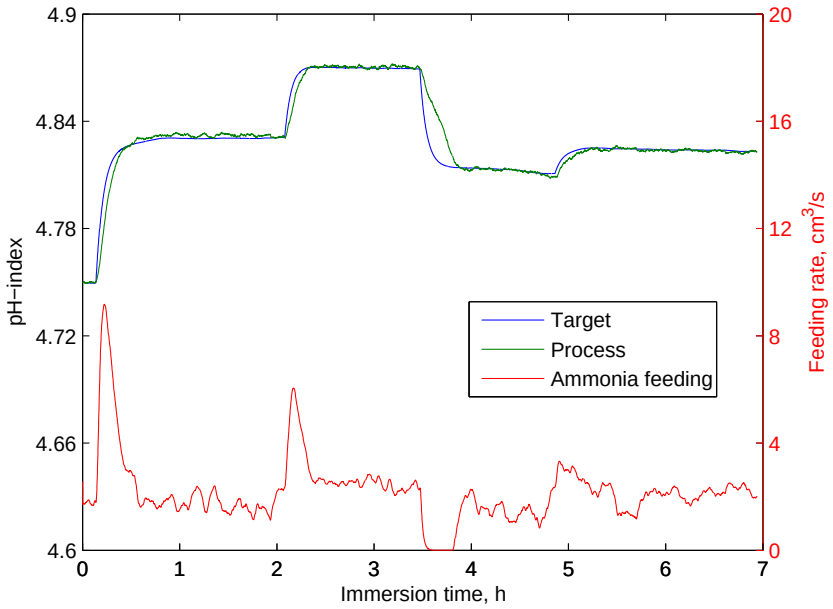

Figure 5.5: Optimal pH and the respective simulated process value with the ammonia addition pumping, used in control.

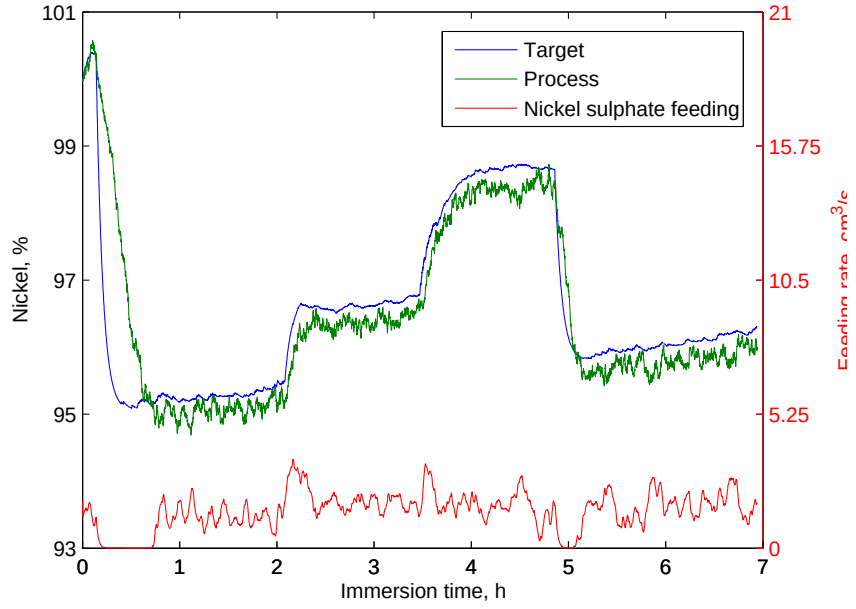

Figure 5.6: Optimal nickel concentration and the respective simulated process value with the nickel sulphate addition pumping, used in control.

is the onesided control. Therefore, the PI-controller is justified and there is no need for a more complex control algorithm. The control concept is also capable of preventing the bath decomposition increasing the bath lifetime to some extent. However, the control is not capable of avoiding bath contamination caused by the solid by-products, which work as a nucleation agent [8, 9, 75]. Therefore, to reach an effective control, a stable process and a uniform product quality, an effective bath agitation and filtering have also to be assured.

5.8 Conclusions

Electroless nickel plating is a widely used method in many applications. In the traditional applications, the alloy properties are not critical and no accurate process control is needed. However, in new applications like in printed circuit board manufacturing the requirements for the alloy are strict and tolerances tight. Especially thickness and phosphorous content of the electroless nickel alloy affect radically the final quality of the PCB. To control these, the traditional operator based process control is not adequate and a more precise control is required.

In this Chapter a new sophisticated control algorithm for electroless nickel plating process was developed. The algorithm uses the developed process model to calculate the optimal nickel ion concentration and pH trajectories according to the process state and the given reference values of the alloy thickness and phosphorous content. The trajectories are tracked by a PI-controlled pumping of ammonia and nickel sulphate.

The accuracy of the algorithm was evaluated by simulations and shown to be functional. It was capable of eliminating the effect of disturbances produced by unstable loading and inaccurate process measurements. It balanced the nickel alloys thickness and phosphorous content at the desired levels and avoided the spontaneous bath decomposition, caused by the unbalance of reactants.

It was also shown, that the alloy thickness and its phosphorous content of an electroless plating can be controlled by controlling the pH and nickel on concentration of the plating bath. This control concept allows separate control of the alloy thickness and phosphorous content abrogating the disagreement between the control of these two parameters, which exists if only a single, pH control is applied.

The proposed control algorithm offers a sophisticated and totally new kind of approach for the control of the electroless nickel process. Its capability to control the alloy thickness and phosphorous content independently, based on the state of the plating bath, offers remarkable improvements for the current control concepts of the electroless plating industry. Because of the proposed control, not only the quality of the plated film can be improved, but also the process conditions can be

optimized and bath contamination avoided, which enable the longer bath lifespan. Therefore, it can be stated, that the quality of the alloy and effectiveness of the plating process can be improved considerably by the proposed control. However, the control concept has been tested only by simulation, not in a real industrial plating process, which would enable better validation of the concept. Despite this, it has been shown, that the proposed control concept has a potential for a real industrial application.

Chapter 6

Conclusions

The electroless nickel plating is a widely used plaiting method in various industrial applications including PCB manufacturing where it is used as a part of ENIG surface finish as a diffusion barrier between coppered circuitry and golden surface layer. In this thesis, a new model along with a method for the control and estimation of a electroless nickel plating process is developed.

The thesis is current, because ENIG is one of the lead-free surface finishes used in PCB manufacturing and in EU area the use of lead in electronic products is restricted by legislation starting from 1.7. 2006. Therefore, it is likely that ENIG will become more common surface finish in the future. However, there is some critical problems involved in the electroless nickel process of ENIG finish which restrict the use of ENIG in PCB manufacturing.

It is well-known that the alloy thickness and its phosphorous content have a dramatic effect on the characteristics of electroless nickel deposit. In PCB manufacturing these affect especially solderability and corrosion resistance of the PCB surface which are critical for the final quality of the PCB. Therefore the alloy thickness and phosphorous content should be controlled during the plating, which is difficult because lack of real-time measurements.

The developed novel model for electroless nickel plating process is based on electrochemical reaction mechanism and mixed potential theory. In addition, the Buttler-Volmer equation, Nernst equations and mass balance are used for the modelling of current densities, equilibrium potentials and concentration dynamics, respectively. Because the model is developed primarily for the ENIG process of PCB manufacturing industry, its input consists of the standard online measurements of the PCB industry. From these, the model produces accurate realtime estimates *inter alia* for alloy thickness, phosphorous content, by-product concentrations and current densities of partial reactions. Based on these estimates, a new monitoring and control system is developed for the process.

The developed model has been tested against independent data gathered from three active and several passive experiments conducted in an industrial PCB manufacturing line. In addition to these experiments shown in the thesis, the model has been former validated with two different industrial plating chemistries from different manufacturers. In all the experiments, the model shows good agreement with the data and correct response to the changes in plating conditions. Therefore, it can be stated that the proposed model is capable of estimating the unobservable product and bath parameters accurately from standard measurements of the PCB industry.

The complicated reaction mechanism of electroless nickel plating reaction is discussed and explained mathematically in the thesis by using the model. This new perspective is in a good agreement with the literature and former research results.

The model is applied in model-based monitoring of an industrial plating process. The monitoring system is shown to be capable of estimating online the same data that is normally measured afterwards in the laboratory analysis. In addition, it provides estimates of alloy's phosphorous content and electrochemical parameters, which are critical for the effective process control, but unfortunately unobservable in normal process control. This information can be used for fast failure detection and corrections in the PCB manufacturing line.

Based on the model, a new sophisticated control algorithm for the plating process is developed. Using the model, the algorithm calculates the optimal nickel ion concentration and pH trajectories according to the given reference values of the alloy thickness and phosphorous content. These trajectories are tracked by PI-controlled pumping of ammonia and nickel sulphate. The accuracy of the control algorithm was evaluated by simulations and shown to be functional being capable of eliminating the effect of disturbances produced by unstable loading and inaccurate process measurements. It balanced the nickel alloy's thickness and phosphorous content at the desired levels and avoided the spontaneous bath decomposition, caused by the unbalance of reactants.

It is also shown, that the alloy thickness and its phosphorous content of an electroless plating can be controlled by controlling the pH and nickel on concentration of the plating bath. This new control concept allows separate control of the alloy thickness and phosphorous content abrogating the disagreement between the control of these two parameters, which exists if only a single, pH control is applied. This is a remarkable improvement for the current control concepts of the electroless plating industry.

In this thesis, it has been shown that the developed monitoring and control algorithms are promising tools for a better control of electroless nickel plating process and they have potential also for commercial applications. In the future work, the algorithms have to be implemented in an industrial plating line for an online use which would enable better validation in a real process environment including pos-

sible exceptions from a normal conditions and process errors. This would reveal their potential weaknesses and validate their usability in industry.

During the research, the adaptation of the developed modelling, monitoring and control principles also to other electroless plating reactions was not studied. However, there seems to be no theoretical restrictions for that, but because the reaction mechanisms and reagents of electroless plating processes differ from each other, the model should not only be calibrated, but also its structure might be needed to be changed. This might not be a problem for several processes, like to electroless copper plating, because of their more simply and well known reaction mechanisms. The applicability of the proposed algorithms would offer effective tools for the process control of many processes in many industries and therefore it is a task to be researched in the future.

In general, the thesis presents a complete view of electroless nickel plating process introducing the basics of the plating reaction, its applications and the previous efforts conducted to develop the process and process control. It also summarizes the main problems related to electroless nickel plating and its control, especially from the PCB industry point of view, and offers several validated novel solutions for these. The proposed methods have a great potential for industrial applications and therefore, the thesis forms a strong basis for the further development of electroless nickel plating process and its control.

Bibliography

[1] Yokomine K., Shimizu N., Miyamoto Y., Iwata Y., Love D., and Newman K. Development of electroless Ni/Au plated build-up flip chip package with highly reliable solder joints. In *Proc. IEEE Electronic Components and Technology Conference*, 2001.

[2] Bradley E. and Banerji K. Effect of PCB finish on the reliability and wettability of ball grid array packages. *IEEE Transactions on Components, Packaging, nd Manufacturing Technology*, 19(2):320–330, 1996.

[3] Kantola K. Modelling of electroless nickel plating process for control purposes. Master's thesis, Helsinki University of Technology, Espoo, Finland, 2004.

[4] Kantola K. Modelling, monitoring and controlling electroless nickel plating process of plated through hole boards. In *Proc. 19th. ECMS*, pages 679–684, Riga, Latvia, 2005.

[5] Nuzzi F. J. Automatic control of electroless nickel plating. *Metal Finishing*, pages 31–33, 1983.

[6] Chen L., Crnic M., Lai Z., and Liu J. Process development and adhesion behaviour of electroless copper on liquid crystal polymer (LCP) for electronic packaging application. *IEEE Transactions on Electronic Packaging Manufacturing*, 25(4):273–278, 2002.

[7] Gawrilow G.G. *Chemical (electroless) Nickel-Plating.* Portcullis Press Ltd., Redhill, United Kindom, 1979.

[8] Schlesinger M. Electroless deposition of nickel. In M. Schlesinger and M. Paunovic, editors, *Modern Electroplating*, pages 667–684. Wiley and Sons, New York, United States, fourth edition, 2000.

[9] Mallory G.O. Electroless plating: fundamentals and applications. In Mallory G.O. and Hajdu J.B., editors, *The fundamental aspects of electroless nickel plating*, pages 1–56. AESF Society, Orlando, United States, 1990.

[10] Putten A.M.T. and Bakker J.W.G. Geometrical effects in the electroless metallization of fine patterns. *J. Electrochem. Soc.*, 140:2221–2228, 1993.

[11] Hamano T. and Ikemoto Y. Electrical characterization of a 500 MHz frequency EBGA package. *IEEE Transactions on Advanced Packing*, 24(4):534–541, 2001.

[12] Keller C.G. and Howe R.T. Nickel-filled hexsil termally actuated tweezers. In *Tech. Dig. Papers, Int. Conf. Solid-State Sensors and Actuators, Transducers '95*, pages 376–379, Stockholm, Sweden, 1995.

[13] Guan S., Nelson B.J., and Vollmers K. Electrochemical codeposition of magnetic particle-ferromagnetic matrix composites for magnetic MEMS actuator applications. *J. Electrochem. Soc.*, 151(9):C545–C549, 2004.

[14] Coombs C.F. Jr. *Printed Circuit Handbook*. McGraw-Hill, New York, United States, 5 edition, 2001.

[15] Dennis J. K. and Such T.E. *Nickel and Chromium Plating*. Butterworths, London, United Kindom, second edition, 1986.

[16] Weil R., Lee J.H., Kim I., and Parker K. Comparison of some mechanical and corrosion properties of electroless and electroplated nickel-phosphorous alloys. *Plating and Surface Finishing*, pages 62–66, 1989.

[17] Huang Y.S., Zeng X.T., Hu X.F., and Liu F.M. Corrosion resistance properties of electroless nickel composite coatings. *Electrochemica Acta*, 49:4313–4319, 2004.

[18] Lin W.L. and Wu C.-H. Structural evolution of electroless nickel bump. *J. Electrochem. Soc.*, 150(5):C273–C276, 2003.

[19] Djokic S. S. Electroless deposition of metals and alloys. In *Modern aspects of electrochemistry*, pages 51–131. Kluwer Academic/Plenum Publishers, London, United Kindom, 2002.

[20] O'Sullivan E. J. Fundamentals and practical aspects of the electroless deposition reaction. In Alkire R. J. and Kolb D. M., editors, *Advances in Electrochemical Science and Engineering*, pages 225–273. Wiley-VCH, Verlag GmbH, Weinheim, Germany, 2002.

[21] Baudrand D. W. Electroless nickel plating. In *ASM Handbook*, pages 290–309. ASM International, 1994.

[22] Kwok R.W.M., Chan K.C.M., and Bayes M.W. Development of an electroless nickel immersion gold process for PCB final finishes. *Circuit World*, 30(3):37–42, 2004.

[23] Lewis D.B. and Marshall G.W. Investigation into the structure of electrodeposited nickel-phosphorous alloy deposition. *Surface and Coating Technology*, 78:150–156, 1996.

[24] European Parliament. *Directive 2002/96/EC of the European Parliament and of the council on Waste of Electrical and Electronic Equipment WEEE*, January 2003.

[25] European Parliament. *Directive 2002/95/EC of the European Parliament and of the council on the Restriction of the use of Hazardous Substances in Electronic and Electronic Equipmant RoHS*, January 2003.

[26] European Commission. *Commission decision 2005/618/EC amending directive 2002/95/EC of the European Parliament and of the Council for the purpose of establishing the maximum concentration values for certain hazardous substances in electrical and electronic equipment*, August 2005.

[27] Crouse K. and Cullen D. A key failyre mode resulting in INTERFACIAL FRACTURE of soldered ENIG surfaces. *Printed Circuit Fabrication*, 25(2):22–32, 2002.

[28] Goosey M. Factors influencing the formation of "black pad" in electroless nickel-immerion gold solderable finishes – a processing perpective. *Circuit World*, 28(3):36–39, 2002.

[29] Jang J.W., Kim P.G., Tu K.N., and Frear D.R. Crystallization of electroless Ni-P under bump metallization induced by solder reaction. In *Proc. IEEE International Symposium on Advanced Packing Materials*, pages 252–255, 1999.

[30] Jeon Y.-D. and Paik K.-W. Stresses in electroless Ni-P film for electronic packaging applications. *IEEE Transactions on Component and Packing Technologies*, 25(1):169–173, 2002.

[31] Brenner A. and Riddell G. Nickel plating on steel by chemical reduction. *J. Res. Nat. Bur. Std.*, 37(31):31–34, 1946.

[32] Brenner A. and Riddell G. Deposition of nickel and cobalt by chemical reduction. *J. Res. Nat. Bur. Std.*, 39(385):385–395, 1947.

[33] Salvago G. and P.L. Cavallotti. Characteristics of the chemical reduction of nickel alloys with hypophosphite. *Plating*, pages 665–671, 1972.

[34] Bindra P. and J.R. White. Fundamental aspects of electroless copper plating. In Hajdu J.B. Mallory G.O., editor, *Electroless plating: fundamentals and applications*, pages 290–329. AESF Society, Orlando, United States, 1990.

[35] Kim Y.-S. and Sohn H.-J. Mathematical modelling of electroless nickel deposition at steady state using rotating disk electrode. *J. Electrochem. Soc.*, 143(2):505–509, 1996.

[36] Paunovic M. and Sclesinger M. *Fundamentals of electrochemical deposition.* John Wiley & Sons, Inc., 1998.

[37] Riedel W. *Electroless Nickel Plating.* Finishing Publications LTD., Hertfordshire, England, 1991.

[38] Abrantes L. M., Oliveira M.V., and Vieil E. A probe beam deflection study of the hypophosphite oxidation on a nickel electrode. *Electrochimica Acta*, 41(10):1703–1711, 1996.

[39] Mital C. K., Shivastava P. B., and Dhaneshwar R. G. *Metal Finishing*, 85(6):31–33, 1987.

[40] Brenner A. *Electrodeposition of Alloys, Principles and Practices.* Academic Press, New York, United States, 1963.

[41] Gorbunova K.M. and Polukarow Y. M. In Tobias C. W., editor, *Advances in Electrochemistry and Electrochemical Engineering.* Interscience, New York, 1967.

[42] White R. E. and Lorimer S. E. A model of the bromine/bromide electrode reaction at a rotating disk electrode. *J. Electrochem. Soc.*, 130:1096–1102, 1983.

[43] White R. E., Lorimer S. E., and Darby R. Predicting of the current density at an elctrode at which multible electrode reactins occur under potentiostatic control. *J. Electrochem. Soc.*, 130:1123–1126, 1983.

[44] Adanuvor P.K., White R., and Lorimer S.E. Modeling the rotating disk electrode for studying the kinetics of electrochemical reactions. *J. Electrochem. Soc.*, 134:625–630, 1987.

[45] Carbajal C. S. and White R.E. Electrochemical production and corrosion testing of amorphous Ni-P. *J. Electrochem. Soc.*, 135(12):2952–2957, 1988.

[46] Yin X., Hong L., Chen B.-H., and Ko T.-M. Modeling the stability of electroless plating bath - diffusion of nickel colloidal particles from the plating frontier. *J. Colloid and Interface Science*, 262:89–96, 2003.

[47] Touhami W.E., Chassaing E., and Cherkaoui M. Modelisation of Ni-P electroless deposition in ammoniacal solutions. *Electrochemica Acta*, 48:3651–3658, 2003.

[48] Newman J. and Tiedemann W.H. Porous-electrode theory with battery applications. *AIChE J. Control and Optim.*, 21(1):25–41, 1975.

[49] Gu H., Nguyen T.V., and White R.E. A mathematical model of a lead-acid cell: Discharge, rest and charge. *J. Electrochem. Soc.*, 134(12):2953–2960, 1987.

[50] Cavalotti P. and Salvago G. Chemical reduction of nickel and cobalt by hypophosphite. *Electrochimica Metallorum*, 1(3):23–41, 1968.

[51] Tenno R., Kantola K., and Tenno A. Electroless nickel plating process model for plated-through-hole board manufacturing. *J. Electron. Mater.*, 35(10):1825–1836, 2006.

[52] Mu H., Seok J., and Lin R.Y. Nickel thin film coatings on steel with electroless plating and sputter deposition. *J. Electrochem. Soc.*, 150(2):C67–C72, 2003.

[53] Tenno R. and Koivo H. State estimation and bath control for the electroless nickel-plating process. In *Proc. European Control Conf.*, Cambridge, United Kindom, 2003. CD-format.

[54] Ramasubramanian M., Popov B.N., White R.E., and Chen K.S. A mathematical model for electroless copper deposition on planar substrates. *J. Electrochem. Soc.*, 146(1):111–116, 1999.

[55] Milazzo G. and Caroli S. *Tables of standard electrode potentials project of the IUPAC electrochemistry commission.* Chichester, New York, United States, xvi edition, 1978.

[56] Tenno R., Kantola K., and Koivo H. Electroless nickel plating: Pcb process modeling and estimation. In *Proc. AIChE Annual Meeting*, Austin, Texas, 2004. CD-format.

[57] Jiaqiang G., Yating W., Lei L., Bin S., and Wenbin H. Crystallization temperature of amorphous electroless nickel-phosphorous alloys. *Material Letters*, 59:1665–1669, 2005.

[58] Kumar P.S. and Nair P.K. Studies on crystallization of electroless Ni-P deposits. *J. Materials Processing Technology*, 56:511–520, 1996.

[59] Krolikowski A. and Wiecko A. Impedance studies of hydrogen evolution on Ni-P allys. *Electrochimica Acta*, (47):2065–2069, 2002.

[60] Kantola K., Tenno R., and Koivo H. Model for electroless nickel plating of through holes board: Model accuracy testing. In *Proc. 5th. IASTED Conf. MSO*, Oranjestad, Aruba, 2005. CD-format.

[61] Tenno R. and Kantola K. Bath and deposit monitoring system for electroless nickel plating process of plated-through-hole board manufacturing. *J. Manufacturing Science and Engineering*, (Submitted).

[62] Gould A.J., Boden P.J., and Harris S.J. Phosphorous distribution in electroless nickel deposits. *Surface Technology*, 12(1):93–102, 1981.

[63] Pfisterer H-C. Data-based modeling of electroless nickel plating. Master's thesis, Helsinki University of Technology / University of Stuttgart, Espoo, Finland / Stuttgart, Germany, 2006.

[64] Ylen J-P. *Measuring, modelling and controlling the pH Value and The Dynamic Chemical State*. PhD thesis, Helsinki University of Technology, Espoo, Finland, 2001.

[65] Xu H., Brito J., and Sadik O.A. Mechanism of stabilizer acceleration in electroless nickel at wirebond substrates. *J. Electrochem. Soc.*, 150(11):C816–C822, 2003.

[66] Malecki A. and Micek-Ilnicka A. Electroless nickel plating from acid bath. *Surface and Coating Technology*, 123:72–77, 2000.

[67] Yi S.H., Von Preissig F.J., and Kim E.S. Electroless nickel films: Properties and fabricated cavity structure. *J. Micromechanical Systems*, 11(4):293–301, 2002.

[68] Cheong W.J., Luan B.L., and Shoesmith D.W. The effects of stabilizers on the bath stability of electroless ni deposition and the deposit. *Applied Surface Science*, 229:282–300, 2004.

[69] Lu G. and Zangari G. Study of the electroless deposition process of Ni-P-based ternary alloys. *J. Electrochem. Soc.*, 150(11):C777–C786, 2003.

[70] Kuczma J.J. Jr. Equipment desing for electroless nickel plating. In Mallory G.O. and Hajdu J.B., editors, *Electroless Plating: Fundamentals and Applications*, pages 139–167. American Electroplaters and surface Finisher Society, Florida, United States, 1990.

[71] Ricky Lee S.-W., Yan C.C., Karim Z., and Huang X. Assesment on the effect of electroless nickel plating on the reliability of solder ball attachment to the bond pads of pbga substrate. In *Proc. IEEE Electronic and Technology Conference*, pages 868–873, 2000.

[72] Jappes J.T.W., Ramamoorthy B., and Nair P.K. A study on the influence of process parameters on effiency and crystallinity of electroless Ni-P deposit. *J. Materials Processing Technology*, 2005.

[73] Tenno R., Kantola K., and Koivo H. Electroless nickel plating: Bath control. In *Proc. 16th IFAC World Cong.*, Praha, Czech Rep., 2005. CD-format.

[74] Oraon B., Majumbar G., and Ghosh B. Application of responce surface method for predicting electroless nickel plating. *Materials and Desing*, 2005.

[75] Tatchev D., Kranold R., and Armyanov S. Characterization of amorphous Ni-P coating by small angle X-ray scattering. *J. Electrochem. Soc.*, 150(7):C502–C506, 2003.

[76] Tenno R., Kantola K., and Tenno A. Incomplete data supervisor control for electroless nickel plating process. *IFAC J. Process Control*, (Submitted).

HELSINKI UNIVERSITY OF TECHNOLOGY CONTROL ENGINEERING LABORATORY

Editor: H. Koivo

Report 136 Zenger, K.
Modelling, Analysis and Controller Design of Time-Variable Flow Processes. March 2003.

Report 137 Hasu, V.
Adaptive Beamforming and Power Control in Wireless Communication Systems. August 2003.

Report 138 Haavisto, O., Hyötyniemi, H.
Simulation Tool of a Biped Walking Robot Model. March 2004.

Report 139 Halmevaara, K., Hyötyniemi, H.
Process Performance Optimization Using Iterative Regression Tuning. April 2004.

Report 140 Viitamäki, P.
Hybrid Modeling of Paper Machine Grade Changes. May 2004.

Report 141 Pöyhönen, S.
Support Vector Machine Based Classification in Condition Monitoring of Induction Motors. June 2004.

Report 142 Elmusrati, M. S.
Radio Resource Scheduling and Smart Antennas in Cellular CDMA Communication Systems. August 2004.

Report 143 Tenno, A.
Modelling and Evaluation of Valve-Regulated Lead-Acid Batteries. September 2004.

Report 144 Hyötyniemi, H.
Hebbian Neuron Grids: System Theoretic Approach. September 2004.

Report 145 Hyötyniemi, H. (ed.)
Complex Systems: Science at the Edge of Chaos - Collected papers of the Spring 2003 postgraduate seminar. October 2004.

Report 146 Paanasalo, J.
Modelling and Control of Printing Paper Surface Winding. June 2005.

Report 147 Mohamed, F.
Microgrid Modelling and Simulation. March 2006.

Report 148 Mäenpää, T.
Robust Model Predictive Control for Cross-Directional Processes. May 2006.

Report 149 Kantola, K.
Modelling, Estimation and Control of Electroless Nickel Plating Process of Printed Circuit Board Manufacturing. March 2006.

ISBN-13 978-951-22-8440-5

ISBN-10 951-22-8440-5

ISSN 0356-0872

Picaset Oy, Helsinki 2006